AIP | The Journal of Chemical Physics

Medium decoupling of dynamics at temperatures ~100 K above glass-transition temperature: A case study with (acetamide + lithium bromide/nitrate) melts

Biswajit Guchhait, Snehasis Daschakraborty, and Ranjit Biswas

Citation: The Journal of Chemical Physics **136**, 174503 (2012); doi: 10.1063/1.4705315
View online: http://dx.doi.org/10.1063/1.4705315
View Table of Contents: http://scitation.aip.org/content/aip/journal/jcp/136/17?ver=pdfcov
Published by the AIP Publishing

Medium decoupling of dynamics at temperatures ~100 K above glass-transition temperature: A case study with (acetamide + lithium bromide/nitrate) melts

Biswajit Guchhait, Snehasis Daschakraborty, and Ranjit Biswas[a)]
Department of Chemical, Biological and Macromolecular Sciences, S. N. Bose National Centre for Basic Sciences, Block-JD, Sector-III, Salt Lake, Kolkata-700098, India

(Received 28 November 2011; accepted 6 April 2012; published online 2 May 2012)

Time-resolved fluorescence Stokes shift and anisotropy measurements using a solvation probe in $[0.78CH_3CONH_2 + 0.22\{f\ LiBr + (1\text{-}f)\ LiNO_3\}]$ melts reveal a strong decoupling of medium dynamics from viscosity. Interestingly, this decoupling has been found to occur at temperatures ~50–100 K above the glass transition temperatures of the above melt at various anion concentrations (f_{LiBr}). The decoupling is reflected via the following fractional viscosity dependence (η) of the measured average solvation and rotation times ($\langle\tau_s\rangle$ and $\langle\tau_r\rangle$, respectively): $\langle\tau_x\rangle \propto (\eta/T)^p$ (x being solvation or rotation), with p covering the range, $0.20 < p < 0.70$. Although this is very similar to what is known for deeply supercooled liquids, it is very surprising because of the temperature range at which the above decoupling occurs for these molten mixtures. The kinship to the supercooled liquids is further exhibited via p which is always larger for $\langle\tau_r\rangle$ than for $\langle\tau_s\rangle$, indicating a sort of translation-rotation decoupling. Multiple probes have been used in steady state fluorescence measurements to explore the extent of static heterogeneity. Estimated experimental dynamic Stokes shift for coumarin 153 in these mixtures lies in the range, $1000 < \Delta\nu^t/cm^{-1} < 1700$, and is in semi-quantitative agreement with predictions from our semi-molecular theory. The participation of the fluctuating density modes at various length-scales to the observed solvation times has also been investigated. [http://dx.doi.org/10.1063/1.4705315]

I. INTRODUCTION

It is long-known that short chain aliphatic amides, when mixed with inorganic salts, produce liquids at or near room temperature with a remarkable tendency to supercool.[1–13] Acetamide has been one of the most frequently used amides because of its unique solvating power[14–19] which arises due to the presence of several functional groups, high molecular dipole moment (3.7 D), and fairly large static dielectric constant ($\varepsilon_0 \approx 60$)[17] in molten state (melting point ~353 K, boiling point ~495 K). These interesting solvent properties coupled with a wide thermal window have made molten mixtures of (acetamide + electrolyte) to be used not only as reaction media in chemical industry but also as materials for electrochemical applications at elevated temperatures.[20,21] These molten mixtures (or simply, melts) are characterized by estimated glass transition temperatures (T_g) $\sim 190 < T_g/K < 250$ range,[22–25] and are termed as supercooled mixtures as they remain in the liquid phase at temperatures much below the respective melting temperatures of the constituents. This "supercooling" phenomenon and the associated importance for chemical industry have motivated much of the research on the basic scientific aspects, because developing these melts into useful dielectric materials[13,26] requires deeper understanding of medium structural and transport properties.

Presence of microheterogeneity in solution structure was suggested earlier by viscoelastic,[11,27] ultrasonic,[3,26] nuclear magnetic resonance,[10] and dielectric relaxation (DR)[3,12] experiments with (amide + salt) melts. A model solution structure consisting of salt domains, amorphous amide, and amide interacting with ions was proposed[13] in order to uniformly explain the relaxation characteristics revealed by the above experiments. Most striking of these experimental studies had been the suggestion of colossal (~10^6) static dielectric constant (ε_0) for these melts by the DR measurements[3,12,13,26] performed in the frequency range, $0.1 \leq \nu/Hz \leq 10^6$, which also reported Cole-Cole[28] relaxation processes with a strong stretching exponent (or shape parameter), particularly at the high frequency region, for (CH_3CONH_2 + NaSCN) melt. In addition, depending upon temperature ($265 \leq T/K \leq 311$), extremely slow relaxation times - one varying between ~10 ms and ~0.5 s at the low frequency regime and the other between ~25 ns and ~250 ns at the high frequency regime - characterized the acetamide-thiocyanate melt data.[12] In contrast, similar measurements with (CH_3CONH_2 + CF_3COONa) and (CH_3CONH_2 + $Ca(NO_3)_2$) melts[3] reported that even though the DR data were equally describable by either Cole-Cole or Davidson-Cole[29] processes, spectral characteristics did not deviate much from the conventional Debye description.[30] Interestingly, the diameter of the charged domain, thought to be responsible for the mega-value of ε_0 and formed via ion aggregation, was estimated to be ~10 nm and in equilibrium with two types of amide environments.[3] Further viscoelastic and ultrasonic

a)Author to whom correspondence should be addressed. Electronic mail: ranjit@bose.res.in.

relaxation measurements[27] revealed the proposed aggregation phenomenon was less pronounced for melts containing ions other than Na^+. This variation notwithstanding, microheterogeneity had been a recurrent theme in the early literature while analyzing the experimental results for these melts.

Recent steady state and time-resolved fluorescence spectroscopic studies with some of these melts have suggested that the average ε_0 of these molten mixtures is much smaller than the reported mega-value and, in fact, very similar to that of ambient liquid formamide (FA).[31,32] Average solvation and rotation times, obtained from dynamic Stokes shift and fluorescence anisotropy measurements,[31] have indicated strong solution heterogeneity as these quantities ($\langle\tau_s\rangle$ and $\langle\tau_r\rangle$) exhibited a fractional solution viscosity dependence, $\langle\tau_x\rangle \alpha (\eta/T)^p$, with p much less than unity but larger for $\langle\tau_r\rangle$ than for $\langle\tau_s\rangle$. The fractional viscosity dependence of these quantities and the consequent departure from the conventional Stokes-Einstein (SE)[33] and Stokes-Einstein-Debye (SED)[34] predictions for these melts are reminiscent of environmental as well as translation-rotation decoupling observed in deeply supercooled liquids.[35–41] Furthermore, the microheterogeneity and the longer-ranged interactions (mainly those proportional to r^{-1}, r^{-2}, and r^{-3}, r being the distance between two interacting species)[42] present in these systems jointly render a resemblance with many room temperature ionic liquids (IL) where microscopic inhomogeneity[43–57] and similar electrostatics govern the liquid properties. The closeness between these melts and dipolar ionic liquids is further evidenced when application of a semi-molecular theory that successfully described the Stokes shift dynamics in ILs and (ionic liquid + polar solvent) binary mixtures[58–62] could also semi-quantitatively predict the solvation time scales and dynamic Stokes shift in (CH_3CONH_2 + Na/KSCN) and (CH_3CONH_2 + $Ca(NO_3)_2$) melts.[31,32] It should be recognized here that the agreement between theory and experiments appears due mainly to the domination of the collective solvent polarization fluctuation in polar solvation energy relaxation where details of solvent structure around a dissolved dipolar solute assumes a secondary importance.[63–65] The striking difference, however, is while fluorescence studies with (CH_3CONH_2 + Na/KSCN) mixtures have revealed strong deviation from the SE and SED predictions, ILs show near hydrodynamic description[66] even though both of these different systems are characterized by heterogeneity and similar interactions.

In the present paper we have expanded our fluorescence investigation into the molten mixtures of acetamide with lithium nitrate and bromide of the following general formula $[0.78CH_3CONH_2 + 0.22\{f\,\mathrm{LiBr} + (1\text{-}f)\,\mathrm{LiNO_3}\}]$, where fractions of the anions (bromide, Br^- and nitrate, NO_3^-) have been varied in order to investigate both the mixed anion effects (MAE)[67–72] and the nature of solute-environment interaction. Composition dependence (via varying f_{LiBr} from 0 to 1) of static and dynamic fluorescence characteristics of a dissolved fluorescent probe and temperature effects on them have been investigated to gain further insight into the solute-medium coupling in these supercooled melts. The amide concentration is kept fixed at 0.78 mole fraction because at this composition the mixture remains in the liquid phase[2,5,22] for the temperature range considered, $303 \leq T/K \leq 364$. In addition, density and viscosity data in the same temperature range for these melts have been measured earlier by different authors[23] which also report, apart from the Vogel-Fulcher-Tammann[73] description of temperature dependent transport properties, presence of a moderate MAE for the electrical conductivity. Interestingly, both steady state and dynamic Stokes shifts measured using C153 exhibit non-ideal anion concentration dependence, indicating fluorescence detection of MAE for $[0.78CH_3CONH_2 + 0.22\{f\,\mathrm{LiBr} + (1\text{-}f)\,\mathrm{LiNO_3}\}]$ melts. Extent of heterogeneity, as suggested by the excitation wavelength ($\lambda_{exc.}$) dependence of the fluorescence emission spectrum and the magnitude of p associated with the fractional viscosity dependence, has been found to be more pronounced in these melts than in $[0.75CH_3CONH_2 + 0.25\{f\,\mathrm{KSCN} + (1\text{-}f)\,\mathrm{NaSCN}\}]$ mixtures.[31] This is a result different from earlier suggestion[3,27] that (acetamide + electrolyte) melts containing cation other than Na^+ is relatively less inhomogeneous. As observed in our previous experiments,[31,32] UV-VIS absorption and fluorescence emission characteristics of C153 indicate an average polarity similar to that of liquid formamide at ambient condition, which is much smaller than what was indicated[3,12,13,26] for this kind of melts. Both $\langle\tau_s\rangle$ and $\langle\tau_r\rangle$ in the present measurements increase with Br^- concentration. This follows the mixture composition dependence of η, which, in our measurements, increases with Br^- concentration. Activation energy (E_{act}) estimated from $\langle\tau_r\rangle$ for a given composition has been found to be ~1.5 times larger than that obtained from $\langle\tau_s\rangle$ and the ratio between $E_a(\langle\tau_r\rangle)$ and $E_a(\langle\tau_s\rangle)$ closely follows that between respective p values. In addition, our application of a semi-molecular theory has revealed that the biphasic solvation response observed in these melts originates from the orientational solvent density fluctuations at the collective and nearest neighbor modes, and the isotropic density fluctuations involving the nearest neighbors.

II. EXPERIMENTAL SECTIONS

A. Sample preparation

C153 (laser grade, Exciton) was used without further purification. Another probe, trans-2-[4-dimethylamino)styryl]benzothiazole (DMASBT), whose excited state lifetime is known to be a function of medium viscosity,[74] was used (as received[75]) only to investigate the $\lambda_{exc.}$ dependence of its steady state fluorescence emission at a given composition of these melts. Acetamide (≥99%, SRL, India), lithium nitrate (≥99.5%, SRL, India), and lithium bromide (>99%, Merck Specialities, India) were vacuum-dried (~300 K) for 24 hours before use. Note here that lithium bromide is the most hygroscopic among these three chemicals and becomes liquid if salt grains are exposed to open air for about ~5–10 minutes. Presence of moisture in LiBr may originate from improper drying and exposure to open air during sample preparation at our experimental condition. Therefore, LiBr used in our samples should be correctly designated as $LiBr.xH_2O$, x denoting the unknown

but small amount of water associated with LiBr present in the melt. This is important because presence of water can substantially affect melt viscosity and other dynamical quantities of interest here. Formamide (>99%, Sigma-Aldrich) was used as received. Since a detailed discussion regarding method of sample preparation for experiments with similar molten mixtures is already given in Ref. 31, we do not repeat but only mention that the concentration of C153 in the sample was always regulated at $\leq 10^{-5}$ M. Proper equilibration of the quartz cuvette (1 cm path length) containing sample with the preheated sample chamber (through hot water circulation, Julabo) was ensured before spectral measurements. A few samples were bubbled with dry N_2 gas before data collection but did not produce any difference in data with those collected with the un-bubbled samples. Since phase separation occurs ~5 K below 303 K for a few of these melts and thus spectroscopic measurements were not carried out at $T(K) < 303$. Composition and temperature dependent viscosities of these melts were measured by using an AMVn automated micro-viscometer from Anton Paar (falling ball method).

B. Data collection and analyses for Stokes shift dynamics

Steady state absorption and fluorescence spectra were collected by using, respectively, a UV-visible spectrophotometer (UV-2450, Shimadzu) and fluorimeter (Fluoromax-3, Jobin-Yvon, Horiba). Solvent blanks were subtracted prior to analysis. Time resolved fluorescence measurements were carried out employing the time correlated single photon counting technique based on a system (LifeSpec-ps, Edinburgh Instruments, U.K.) mounted with a laser diode that provides excitation light ($\lambda_{exc.}$) at 409 nm. Time-resolved emission spectra were reconstructed from a series of 18–20 magic angle (54.7°) decays at equally spaced wavelengths across the steady-state emission spectrum of C153 dissolved in molten mixtures.[76] The full width at half maximum (FWHM) of instrument response function (IRF) was ~70 ps. The details regarding fitting of the collected decays have already been discussed elsewhere.[31,76] Solvation response function was constructed as follows:

$$S(t) = \frac{\nu(t) - \nu(\infty)}{\nu(0) - \nu(\infty)}, \tag{1}$$

where $\nu(0)$, $\nu(t)$, and $\nu(\infty)$ denote some measure (usually peak) of frequency for the reconstructed emission spectrum respectively at $t = 0$ (that is, immediately after excitation), at any given instant (t), and at a time sufficiently long ($t = \infty$) to allow for the complete solvent relaxation. By construction, $S(t)$ is a normalized function which decays from unity to zero as the environment rearranges with time in response to the instantaneous alteration of the equilibrium charge distribution of the solute via laser excitation. Note that for a given mixture composition and temperature $\nu(\infty)$ is expected to be equal to the frequency ($\nu_{fl.}$) of the steady state emission spectrum of the solute probe. However, in some cases solvent reorganization during the excited state lifetime of the probe may not be complete, leading to $\nu(\infty) < \nu_{fl}$.[31,77,78] Subsequently, average solvation time ($\langle \tau_s \rangle$) was obtained via analytical integration of the multi-exponential fits to the measured $S(t)$ decay as follows:[79]

$$\langle \tau_s \rangle = \int_0^\infty dt\, S(t) = \int_0^\infty dt \sum\nolimits_i [a_i \exp(-t/\tau_i)] = \sum\nolimits_i a_i \tau_i, \tag{2}$$

where $\sum_i a_i = 1$, and a_i and τ_i, respectively, denote the amplitude and time constant associated with the i-th component of the total decay.

C. Data collection and analyses for time-resolved fluorescence anisotropy

Time-resolved fluorescence anisotropy measurements were carried out, as usual,[80,81] via a set of three decays, magic angle, parallel (I_{para}) and perpendicular (I_{perp}) with respect to the polarization of the excitation light, collected at the peak wavelength of the steady state fluorescence emission spectrum of a probe dissolved in a melt at a given composition and temperature. The magic angle decay was first deconvoluted from the IRF and fitted to a multi-exponential function of time followed by the parallel and the perpendicular decays, and then were simultaneously fitted by using an iterative reconvolution algorithm[82] to generate the anisotropy decays as follows:

$$r(t) = \frac{I_{para}(t) - G I_{perp}(t)}{I_{para}(t) + 2G I_{perp}(t)}, \tag{3}$$

where the geometrical factor (G-factor), determined via tail matching, was found to be 1.2 ± 0.1. $r(t)$ decays, so obtained, were found to fit to bi-exponential function of the following form:

$$r(t) = r(0)[a_1 \exp(-t/\tau_1) + (1 - a_1) \exp(-t/\tau_2)], \tag{4}$$

where τ_i (i = 1, 2) represents the time constants for the decay components (a_i). The value for the initial anisotropy, $r(0)$, was fixed at 0.376 while fitting the $r(t)$ for C153 in all the solutions studied here.[80] The average rotational correlation time $\langle \tau_r \rangle$ was then determined as follows:

$$\langle \tau_r \rangle = \int_0^\infty dt [r(t)/r(0)] = a_1 \tau_1 + (1 - a_1)\tau_2. \tag{5}$$

III. RESULTS AND DISCUSSION

A. Steady state spectral measurements: Heterogeneity signatures

Figure 1 depicts the absorption and emission spectra of C153 in [$0.78CH_3CONH_2$ + $0.22\{f$ LiBr + (1-f) $LiNO_3\}$] melt at $f_{LiBr} = 0.6$ and 303 K, and also those in liquid formamide (broken lines) at the same temperature. The striking resemblance between the spectra in the melt and those in FA ($\varepsilon_0 = 111$)[83] indicates very similar solute-solvent interaction in these two different types of media. Interestingly, the closeness in spectral peak positions alone cannot suggest that ε_0 of this (acetamide + salt) melt is much less than the mega-value reported earlier for similar melts[3,12,13] because in the limit of large ε_0 the transition frequency (absorption or emission) becomes insensitive to the value of average static

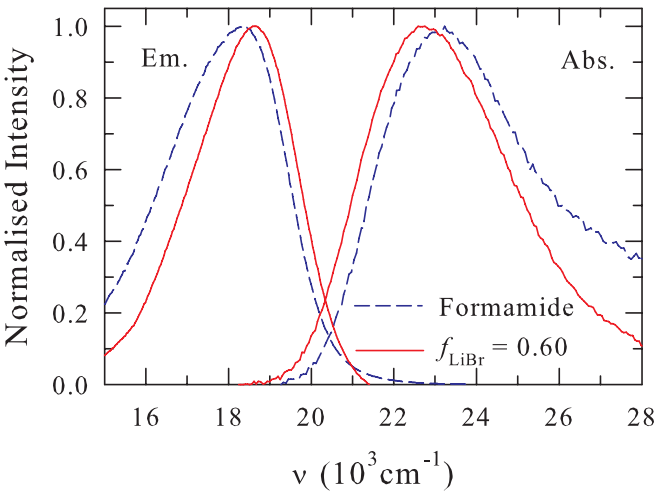

FIG. 1. Representative steady state absorption and emission spectra (color coded) of the dissolved solute (C153) at 303 K in [0.78CH_3CONH_2 + 0.22{*f* LiBr + (1-*f*) $LiNO_3$}] molten mixtures at f_{LiBr} = 0.60 and those in formamide.

dielectric constant. Dynamic Stokes shift measurements and subsequent analyses using a suitable molecular theory, however, may provide a resolution to the debate. Since this issue would be discussed later at length, let us now present results from the steady state spectroscopic measurements revealing more on the equilibrium structural aspects of these molten mixtures.

Figure 2 demonstrates the LiBr concentration (f_{LiBr}) dependence of the steady state absorption and fluorescence emission frequencies (upper panel), the steady state and dynamic Stokes shifts (middle panel) and the difference between them (lower panel) at 303 K and 318 K. Corresponding data for 313 K are shown in Fig. S1 (see supplementary material[84]). Note that the Stokes shift dynamics at ≥318 K is too fast to be measured by our present experiments and thus we show steady state data for these temperatures only. It is interesting to note that while the average absorption frequencies (ν_{abs})[85,86] at both the temperatures exhibit a non-monotonic f_{LiBr} dependence, emission frequencies (ν_{em}) remain largely insensitive to that. The initial blueshift (by ∼200–300 cm^{-1}) of ν_{abs} with f_{LiBr} may arise from the following reasons: (i) reduced availability of acetamide molecules for interacting with the solute (C153) due to solvation of both NO_3^- and Br^- ions, (ii) the variation in packing due to difference in sizes of these solvated anions.[87] The presence of both NO_3^- and Br^- in the melt at this regime increases solution heterogeneity and this is reflected in the f_{LiBr} dependent absorption spectral width shown in Fig. S2 (see supplementary material[84]). Further replacement of NO_3^- by Br^- probably enhances the extent of anion-C153 interaction that induces redshift and thus sets up the observed non-monotonic composition dependence. The heterogeneity in turn becomes less pronounced and consequently the spectral width decreases (see Fig. S2). Since both NO_3^- and Br^- are uni-negative ions, the extent of electrical (ion-dipole) interaction between C153 and these anions is near-equivalent, producing very similar ν_{abs} for binary melts with f_{LiBr} = 0 and f_{LiBr} = 1. Another subtle aspect may be noted in Fig. 2 is that ν_{abs} at f_{LiBr} = 0 is larger at 303 K than

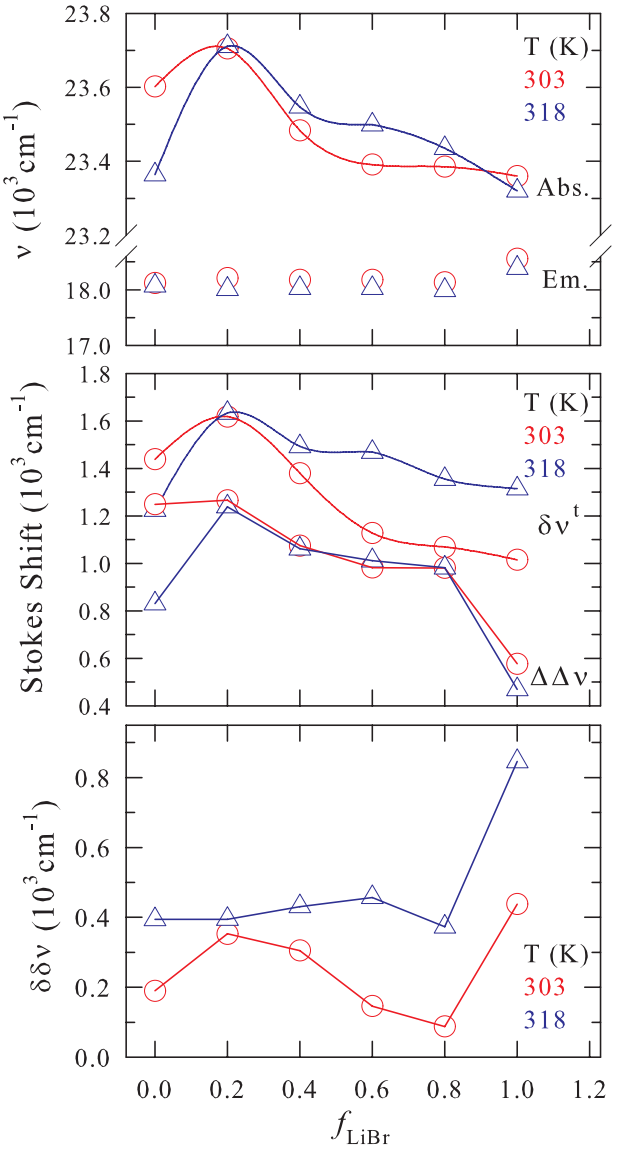

FIG. 2. Composition (f_{LiBr}) dependence of spectral parameters at different temperatures (color coded). While the f_{LiBr} dependent absorption and emission frequencies are shown in the upper panel, steady state relative Stokes' shift ($\Delta\Delta\nu$) and estimated dynamic Stokes' shift ($\Delta\nu^t$) are presented in the middle panel. Lower panel shows the composition dependence of difference between the relative and dynamic shifts, defined as: $\delta\delta\nu = \Delta\nu^t - \Delta\Delta\nu$. The relative Stokes shift has been obtained by using the relation $\Delta\Delta\nu = [\nu_{abs.} - \nu_{em.}]^{mixture} - [\nu_{abs.} - \nu_{em.}]^{heptan\ e} = \Delta\nu^{mixture} - \Delta\nu^{heptan\ e}$ with $\Delta\nu^{heptan\ e}$ = 4230 cm^{-1}, and $\Delta\nu^t = [\nu(t=0) - \nu_{em.}(t=\infty)]^{mixture}$. $\nu(t=0)$ has been obtained by using the Fee-Maroncelli method (Ref. 90). Measured frequencies are better than ±150 cm^{-1} $\delta\nu^t \equiv \Delta\nu^t$.

that at 318 K whereas the temperature-induced variation at f_{LiBr} = 1 is negligible. This difference may be attributed to the relatively less solute-ion interaction at f_{LiBr} = 0 because of higher lattice and gas-phase bond dissociation energies for $LiNO_3$ than that for LiBr.[88] The insensitivity of ν_{em} to mixture composition, also observed earlier for [0.75CH_3CONH_2 + 0.25{*f* KSCN + (1-*f*) NaSCN}] molten mixtures,[31] arises probably due to shorter heterogeneity lifetime than that of fluorescent probe in the excited state.[51,54(a),89] Note ν_{em} in binary melt with f_{LiBr} = 1 at these temperatures are "bluer" than expected and this could be due to relatively slower

environmental relaxation[77,78] because of larger effective (solvated) size and heavier mass of Br^- compared to those of NO_3^-.

The composition dependent steady state Stokes shift ($\Delta\Delta\nu$) and total dynamic Stokes shift ($\delta\nu^t$) estimated[90] from time-resolved data, shown in the middle panel of Fig. 2, clearly indicate that steady state fluorescence emission in these melts occurs from an incompletely solvent-relaxed excited solute. The difference, $\delta\delta\nu = \delta\nu^t - \Delta\Delta\nu$, is positive and ranges between ~100 and 800 cm^{-1} and is similar - both in nonmonotonicity and magnitude - to our earlier results for $[0.75CH_3CONH_2 + 0.25\{f\,KSCN + (1\text{-}f)\,NaSCN\}]$ melts.[31] What is striking though is that the composition dependent $\delta\delta\nu$, shown in the lower panel, is larger at higher temperature ($\delta\delta\nu$ values at 313 K are summarized in Table S3[84]). This suggests increased presence of ions at higher temperature forcing the steady state fluorescence to occur from excited solutes locked in solvent configurations which are far from completely relaxed.

The heterogeneity aspect of these melts is further investigated by following the excitation wavelength ($\lambda_{exc.}$) dependence of the steady state fluorescence emission from two dissolved probes, C153 and DMASBT. In common solvents, the average excited state lifetime ($\langle\tau_{life}\rangle = \sum_i a_i\tau_i/\sum_i a_i$) of DMASBT, a function of both η and ε_0, ranges between 20 and 100 ps[91] and thus significantly shorter than that (3–5 ns)[76] for C153. In addition, collected time-resolved decays (magic angle) of fluorescence emission from DMASBT dissolved in $[0.78CH_3CONH_2 + 0.22\{f\,LiBr + (1\text{-}f)\,LiNO_3\}]$ molten mixture at 303 K with $f_{LiBr} = 0.2$ and 0.8 have been found to fit to bi-exponential function of time, producing ~470 ps and ~600 ps respectively as $\langle\tau_{life}\rangle$ at these compositions (see Fig. S4, supplementary material[84]). Fluorescence signature of DMASBT in these melts would therefore be more responsive to those "shorter-lived" domains which could not be distinguished by the relatively longer-lived excited C153. $\lambda_{exc.}$ dependent emission frequencies ($\nu_{em.}$) for these two fluorophores in $[0.78CH_3CONH_2 + 0.22\{f\,LiBr + (1\text{-}f)\,LiNO_3\}]$ molten mixture at 303 K with $f_{LiBr} = 0.2$ are shown in the upper panel of Fig. 3. Note $\nu_{em.}$ for DMASBT shifts by ~1200 cm^{-1} for changing $\lambda_{exc.}$ from the bluest to the most red of the considered wavelengths, and is nearly double of what C153 exhibits in the equivalent $\lambda_{exc.}$ range. The $\lambda_{exc.}$ dependence of fluorescence spectral width ($\Gamma_{em.}$), shown in the middle panel, also follows the expected trend of narrowing down with increased solvation for both these probes, the extent of total narrowing for DMASBT being approximately thrice as large as that for C153. These results, even though cannot suggest any domain size or the length scale over which medium particles are correlated, do provide an idea about the lifetime of microscopic structures that render spatial heterogeneity in these melts. One of the implications of this finding is that in frequency domain experiments, such as dielectric relaxation spectroscopy, effects of such short-lived structures will probably not be reflected at the megahertz (MHz) region.

Composition dependence of the heterogeneity in $[0.78CH_3CONH_2 + 0.22\{f\,LiBr + (1\text{-}f)\,LiNO_3\}]$ molten mixture at a given temperature is next investigated by monitoring the changes in spectral (emission) position and width for these solutes. Results are summarized in the lower panel of Fig. 3 where the differences between emission frequencies ($\Delta\nu$) and widths ($\Delta\Gamma$) obtained by exciting the solutes at the smallest (bluest, $\lambda_{exc.,b}$) and largest (most red, $\lambda_{exc.,r}$) wavelengths at a given composition and temperature are shown as a function of LiBr concentration, f_{LiBr}. These quantities are defined as follows: $\Delta x(f_{LiBr}, T) = x(f_{LiBr}, T, \lambda_{exc.,b}) - x(f_{LiBr}, T, \lambda_{exc.,r})$ with $x = \nu_{em.}$ or Γ_{em}. Spectral features ($\Delta\nu$ and $\Delta\Gamma$) displayed here have been obtained at $T = 303$ K, and represent the trend observed at few other higher temperatures. It is evident from this panel that the $LiNO_3$-rich solution is more heterogeneous and the extent of heterogeneity decreases upon progressive replacement of NO_3^- by Br^-. In addition, DMASBT reveals more

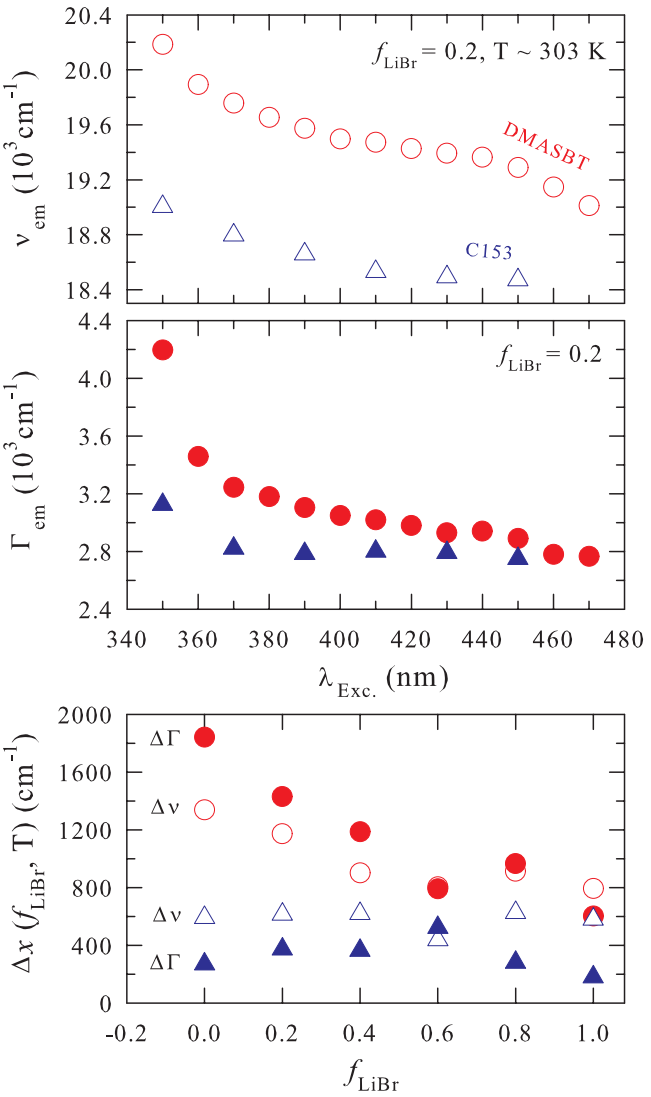

FIG. 3. Excitation wavelength dependence (λ_{exc}) of emission peak frequency (ν_{em}) for DMASBT and C153 (upper panel) and full widths at half maximum (FWHM, Γ_{em}) of emission spectra of these two solutes in $[0.78CH_3CONH_2 + 0.22\{f\,LiBr + (1\text{-}f)\,LiNO_3\}]$ molten mixtures at $f_{LiBr} = 0.2$ and 303 K (middle panel). Composition dependent total differences (Δx) in Γ_{em} and ν_{em} are shown in the lower panel. This is defined as $\Delta x(f_{LiBr}, T) = x(f_{LiBr}, T, \lambda_{exc.,b}) - x(f_{LiBr}, T, \lambda_{exc.,r})$, x being Γ_{em} or ν_{em}. $\lambda_{exc.,b}$ and $\lambda_{exc.,r}$ are the shortest (bluest) and longest (most red) wavelengths used for solute excitation. The uncertainty in frequencies remains the same as in Fig. 2. Widths are better than ±250 cm^{-1}.

pronounced heterogeneity at all compositions than that by C153. The increased heterogeneity in presence of $LiNO_3$ could arise from the presence of both ionic and non-ionic species because of less dissociation of $LiNO_3$ compared to LiBr. Higher lattice and gas-phase dissociation energies[88] for $LiNO_3$ than those for LiBr, and increase in electrical conductivity[23] of the melt upon replacing $LiNO_3$ by LiBr seem to support the above view.

B. Time-resolved measurements: Stokes shift dynamics and relevant density fluctuation modes

As already indicated, characteristics of fluorescence emission intensity decays collected at magic angle for C153 in these mixtures depend upon the detection wavelength, showing signatures of environmental rearrangement with time in response to an instantaneously altered charge distribution of a dissolved solute. A representative example is provided in Fig. 4 where emission decays collected at a shorter wavelength ("blue" with respect to the peak wavelength of the corresponding steady state emission spectrum) and at a longer wavelength ("red") along with their multi-exponential fits, residuals and fit parameters are shown for a melt with f_{LiBr} = 0.6 at 303 K. The presence of decays only at the blue wavelength and both rise and decay at the red wavelength clearly suggest time-dependent solvation of the excited solute in these melts. Note that even though most of the time-resolved emission intensity profiles require tri-exponential functions of time for adequate description, intensity profiles collected around the peak wavelength can be sufficiently represented by a sum of two exponentials. In addition, effects of fluorescence quenching on the detected spectral dynamics have been found to be secondary as the composition dependent longest time constant ($\tau_{Longest}$) associated with the decays at 303, 313, and 318 K, shown in Fig. S5 (see supplementary material[84]), varies by a maximum of ~20%. Therefore, the decay characteristics at various emission wavelengths may be regarded as representing the dynamics of solvation of the excited solute (C153) in these molten mixtures.

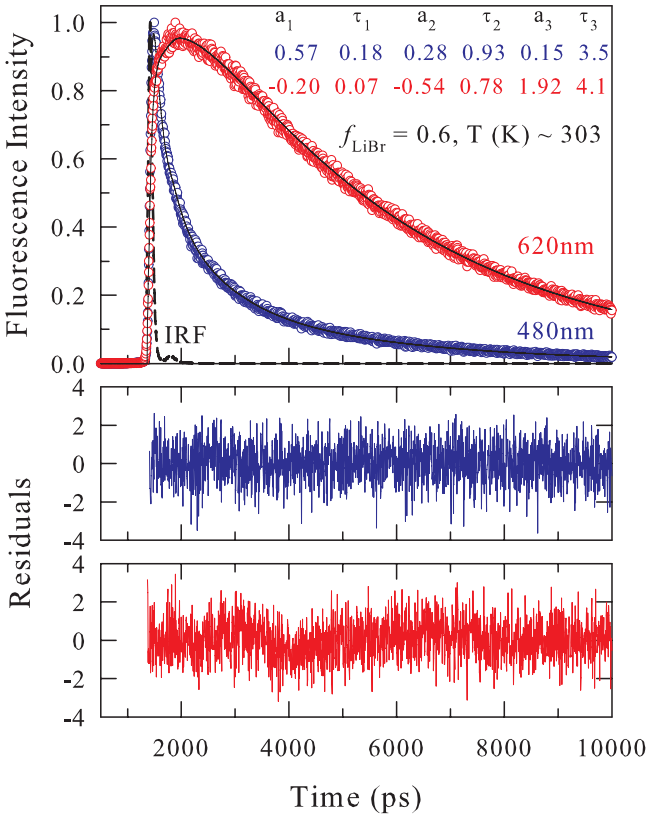

FIG. 4. Representative fluorescence intensity decays at blue (480 nm) and red (620 nm) wavelengths for C153 in molten mixtures at f_{LiBr} = 0.60 and ~303 K. Circles denote the experimental data and solid lines fit through them. Instrument response function (IRF) is also shown in the same figure (dashed lines). The respective residuals (color coded) are presented in the bottom panels. The fit parameters are shown in the inset of the upper panel. Time constants (τ_i) are in the unit of nanosecond. The goodness-of-fit parameters (χ^2) in these two wavelengths are 1.05 and 1.02, respectively.

Time-resolved emission spectra (TRES), obtained via fit through data points using a log-normal line-shape function,[92] are shown in the upper panel of Fig. 5 for C153 in [0.78CH_3CONH_2 + 0.22{*f* LiBr + (1-*f*) $LiNO_3$}] molten mixture along with the corresponding steady state emission spectrum. The results are for f_{LiBr} = 0.6 at 303 K and representative of what have been observed at other compositions as well. Note the steady state emission spectrum and the time-resolved spectrum at $t = \infty$ do not overlap (difference between them being ~300 cm^{-1}) and may indicate incomplete environmental reorganization during the steady state fluorescence emission. The amount of dynamic Stokes shift, $\delta\nu^t = \nu(t=0) - \nu(t=\infty)$, observed at this composition and temperature is ~900 cm^{-1}, which is ~20% less than the estimated[90] shift in case of full detection. The broader time-resolution employed in the present experiments has not only led to the incomplete detection of the total dynamics but also inaccurately captured the evolution of the spectral width at early times. This is shown in the lower panel of Fig. 5 where evolution of the spectral width, $\Gamma(t)$, exhibits opposite trends at early times for melts at f_{LiBr} = 0 and f_{LiBr} = 1. However, $\Gamma(t)$ reaches a plateau as solvation progresses with time, an aspect also observed earlier for polar solvation energy relaxation in neat solvents[76] and molten mixtures.[31,32] This and the fact that even the maximum variation of $\Gamma(t)$ being substantially smaller than the observed dynamic shift further support that the observed time-evolution of the fluorescence spectrum occurs mainly due to the medium reorganization around the perturbed solute in these melts.

Table I summarizes the composition dependent observed ($\Delta\nu^t_{obs.}$) and estimated ($\Delta\nu^t_{est.}$) dynamic Stokes shifts for C153 in these molten mixtures at three different temperatures. These data suggest that approximately 20–50% of the full dynamics, depending upon composition and temperature, has not been detected in the present experiments. Interestingly, even after missing such a significant portion, the observed shift is quite large and lies in the range, ~650–1300 cm^{-1}. The estimated shift, on the other hand, ranges between ~1000 cm^{-1} and 1700 cm^{-1}, and is somewhat smaller than $\Delta\nu^t_{est.}$ for C153 in [0.75CH_3CONH_2 + 0.25{*f* KSCN + (1-*f*) NaSCN}] melts.[31] Reduced ion-solute interaction due to larger effective size[90] of solvated Li^+ ion compared to those for solvated Na^+ and K^+ ions could be one of the reasons behind the difference between the estimated shifts in

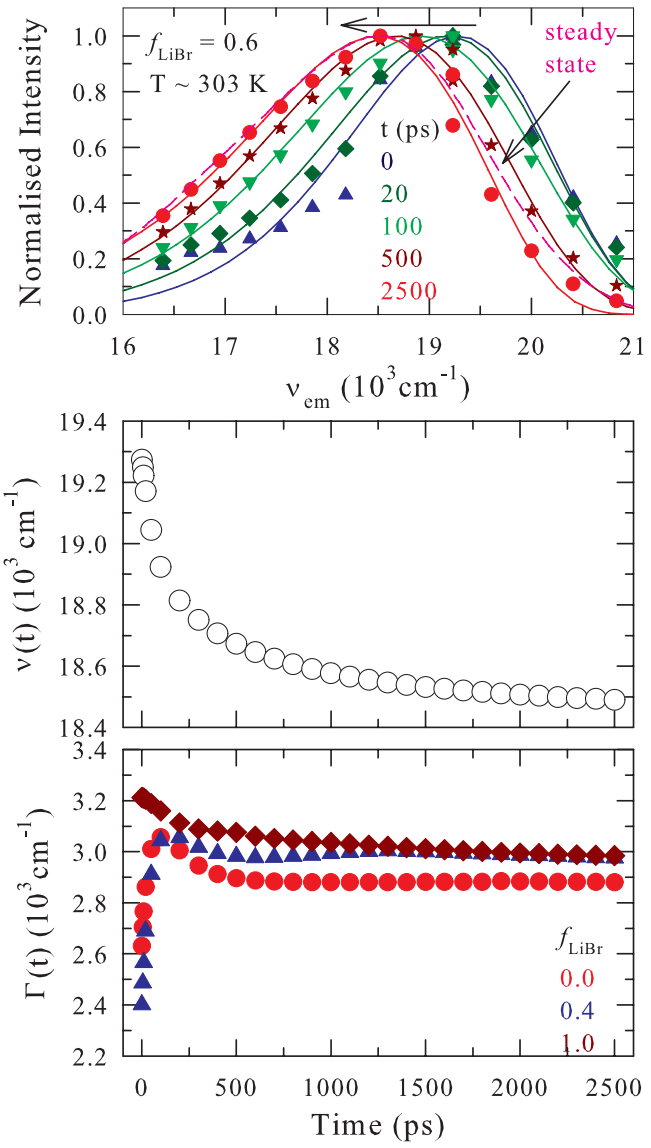

FIG. 5. Synthesized time resolved emission spectra (TRES) of C153 at different time slices from the experimentally obtained decays in [0.78CH_3CONH_2 + 0.22{*f* LiBr + (1-*f*) $LiNO_3$}] molten mixtures at f_{LiBr} = 0.6 and 303 K. TRES shown (upper panel) are at the following time intervals after solute excitation: 0 ps (triangles), 20 ps (diamonds), 100 ps (inverted triangles), 500 ps (asterisk), and 2500 ps (circles). While time evolution of the average peak frequencies ($\nu(t)$) at $f_{LiBr} = 0.6$ is shown in the middle panel, that of the width ($\Gamma(t)$) at three different compositions are shown in the lower panel. For lower panel, circles represent $\Gamma(t)$ for C153 in molten mixture at $f_{LiBr} = 0$, triangles at $f_{LiBr} = 0.4$, and diamonds at $f_{LiBr} = 1.0$.

(CH_3CONH_2 + LiBr/NO_3) and (CH_3CONH_2 + Na/KSCN) molten mixtures. It should be noted that presence of a picosecond component or even a faster one in these mixtures is quite natural because amides and partially substituted amides possess intermolecular libration modes[93,94] centred around 50–100 cm^{-1}, and these collective modes have been shown earlier[95–98] to generate ultrafast polar solvation response in associated molecular solvents. This will be discussed in some detail when we explore the origin of the timescales revealed by dynamic Stokes shift measurements. Let us now focus on understanding the composition dependent dynamic Stokes shift estimated for these mixtures at different temperatures in terms of solute-ion and solute-solvent interactions.

TABLE I. Dynamic Stokes shift of C153 in [0.78CH_3CONH_2 + 0.22{*f* LiBr + (1-*f*) $LiNO_3$)] molten mixtures at 303, 313, and 318 K: Comparison between experiments and theoretical calculations. Uncertainty associated with the measured shift is ±200 cm^{-1}.

	Experiment			Theory		
f_{LiBr}	$\Delta\nu^t_{obs.}$ (cm^{-1})	$\Delta\nu^t_{est.}$ (cm^{-1})	% missed	$\Delta\nu^t_{total}$ (cm^{-1})	$\Delta\nu^t_{sd}$ (cm^{-1})	$\Delta\nu^t_{si}$ (cm^{-1})
			303 K			
0.0	993	1439	31	1727	1147	580
0.2	1305	1619	19	1717	1139	578
0.4	963	1380	30	1705	1129	576
0.6	909	1128	19	1684	1112	572
0.8	847	1069	21	1674	1104	570
1.0	650	1015	36	1658	1091	567
			313 K			
0.0	956	1409	32	1678	1103	575
0.2	1175	1606	27	1667	1094	573
0.4	871	1655	47	1655	1084	571
0.6	1067	1413	24	1641	1073	568
0.8	975	1295	25	1631	1065	566
1.0	844	1265	33	1619	1055	564
			318 K			
0.0	886	1224	28	1656	1083	573
0.2	1042	1634	36	1644	1073	571
0.4	896	1493	40	1633	1064	569
0.6	1057	1469	28	1618	1052	566
0.8	954	1355	30	1607	1044	563
1.0	891	1315	32	1596	1035	561

We follow our earlier model[31,32] in considering the molten mixtures of acetamide with lithium bromide and nitrate as non-aqueous electrolyte solutions where ions, from complete dissociation of the added salts, are dispersed in dipolar solvent, acetamide. In an extremely dilute solution of a solute probe (concentration $\leq 10^{-5}M$) in such a multicomponent mixture, an equilibrium is established mainly via solute-solvent dipolar interaction and solute-ion dipole-ion interaction in addition to ion-ion, ion-solvent, and solvent-solvent interactions. Probe-probe interaction is believed negligible because of its presence at extreme dilution, and interactions between particles (solvent-solvent, ion-ion and ion-solvent) are considered unchanged in presence of solute molecules at this dilution. In such a model, the solute-medium total interaction energy can be approximated to be composed of solute-solvent dipole-dipole interaction and solute-ion dipole-ion interaction. Note in real mixtures salts are not always completely dissociated and various complex entities, such as ion-pairs, triple ions and neutral triple ions,[99–102] exist, and contribute to some extent to the solution energetics and dynamics. However, solute-solvent (dipole-dipole) and solute-ion (dipole-ion) interactions are expected to be the dominant contributors to the dynamic Stokes shift in these (acetamide + salt) melts and hence contributions from more complex species are considered to be of secondary importance. In addition, acetamide molecule is assumed to be spherical with point dipole at the centre, and characterized by a diameter, σ = 4.52 Å (obtained from van der Waals volume[103]) and a dipole moment,[17] μ = 3.7*D*. Ions (both

cation and anion) are treated as hard spheres with central point charges with diameters (σ_i) 1.8 Å[104] for Li^+, 3.92 Å[105] for NO_3^- and 3.64 Å[104] for Br^-. Note here that NO_3^- is not spherical and the actual shape of this ion and other species may have some effects on probe solvation and rotation dynamics. Since the main focus of the present treatment is to understand, at best qualitatively, the observed dynamics in these complex systems in terms of simple microscopic picture, we have avoided considerations of shape asymmetry and medium inhomogeneity while obtaining the static correlation functions. This is done to preserve the analytical simplicity of the theoretical treatment. As before,[31] the composition dependent ε_0 at a particular temperature has been calculated by using the experimental density and dipole moment (3.7 D) in a relation given by the mean spherical approximation (MSA) theory.[106] The calculated composition dependent ε_0, depicted in Fig. S6 (see supplementary material[84]), is ∼30 for these molten mixtures. Parameters used to characterize the solute are the diameter for C153 (7.8 Å) and its excited state dipole moment (14 D).[76] Necessary equations for the calculations of dynamic Stokes shift are provided in the supplementary material[84] (A1), details of which can be found elsewhere.[31,59–62] We only state here that orientational solvent-solvent direct correlation function and static structure factor, required for the calculations,[31] have been obtained from the MSA theory, and the solute-ion static correlations from our earlier works.[59–62] The average spatial arrangement of ions (static ion structure factor) in such mixtures has been obtained by following the method as described previously.[107–109]

Calculated composition dependent dynamic Stokes shifts ($\Delta\nu^t_{total}$) at 303 K, 313 K and 318 K are summarized in Table I along with the solute-solvent dipole-dipole and solute-ion dipole-ion interaction contributions, $\Delta\nu^t_{sd}$ and $\Delta\nu^t_{si}$, respectively. Note the calculated total shift ($\Delta\nu^t_{total}$) spans rather a narrow range (∼1600–1700 cm^{-1}) and similar to the range of estimated shift from experiments ($\Delta\nu^t_{est}$) at these temperatures, 1300–1800 cm^{-1}. This is an important result because a model calculation with ε_0 as moderate as ∼30 could produce such a close agreement with experimental estimates for these molten mixtures whose dielectric constants are supposed to be colossal. The agreement also indicates the validity of the present model that dynamic shift in these molten mixtures could be expressed in terms of solute-medium dipole-dipole and dipole-ion interactions without much adherence to the solution structural complexity. The dipole-dipole interaction contributes ∼65% to the total shift in all these melts and thus dominates over the solute-ion (dipole-ion) contribution. A close inspection of these data also indicates a linear decrease of the calculated shift with composition, the maximum decrease being ∼4% for the total calculated shift, ∼5% and ∼2% respectively for the dipole-dipole and dipole-ion contributions. Even though mass density of the melt increases upon addition of LiBr in the melt,[23] a decrease in number densities of both the dipolar and ionic species (see Fig. S7, supplementary material[84]) reduces the interaction contributions. Note, however, that experimental estimated shifts show a non-linear composition dependence and the extent of variation is much larger (∼30–45%) than the decrease in calculated shifts. The non-linearity is absent in the calculations probably because of the neglect of specific solute-ion interaction, solution heterogeneity and interactions between the solute and other complex ionic species present in these melts.

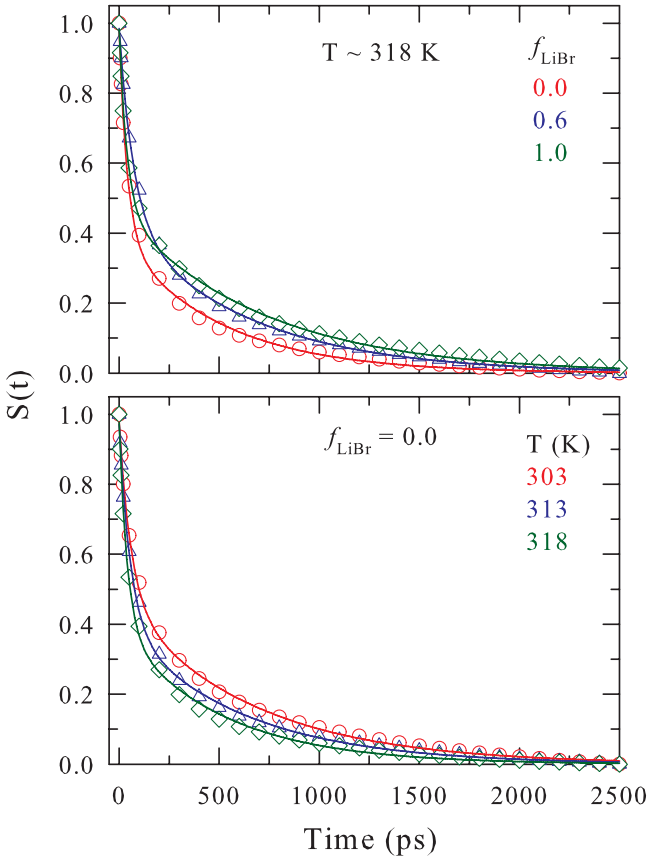

FIG. 6. Decays of solvation response function, $S(t)$, measured using C153 at 318 K in $[0.78CH_3CONH_2 + 0.22\{f\,LiBr + (1\text{-}f)\,LiNO_3\}]$ molten mixtures at $f_{LiBr} = 0.0$ (red), 0.6 (blue), and 1.0 (green) are shown in the upper panel. Temperature effects are shown in the lower panel by presenting $S(t)$ decays at three different temperatures, 303 K (red), 313 K (blue), and 318 K (green), for C153 in the molten mixture with composition $f_{LiBr} = 0.0$.

The dependences of the measured solvation response function, $S(t)$, on mixture composition and temperature are depicted in Fig. 6 where $S(t)$ decays at three different compositions at 318 K are shown in the upper panel, and those at different temperatures at a fixed composition ($f_{LiBr} = 0$) in the lower panel. Both the composition and temperature dependent decays follow the changes in solution viscosity (η) as the latter, summarized in Table S8 (see supplementary material[84]), increases upon increasing LiBr concentration in the melt at a fixed temperature and a decreases upon raising the solution temperature at a fixed composition. Note here that η measured by us increases with LiBr concentration at a fixed temperature which is opposite to the trend reported in Ref. 23. As already mentioned, presence of substantial amount of moisture in LiBr might have led to the erroneous trend reported in Ref. 23. Note in the lower panel that even the slowest of the decays (the one at 303 K) continues only up to 2.5 ns. Such a shorter time-spread for $S(t)$ decays in these melts is unexpected. The reason is the following. According to continuum model, solvation time correlation function for a dipolar solute in a polar continuum is single exponential characterized by a time constant,[110] $\tau_L = \frac{(2\varepsilon_\infty+\varepsilon_c)}{(2\varepsilon_0+\varepsilon_c)}\tau_D \approx \frac{(\varepsilon_\infty+1)}{(\varepsilon_0+1)}\tau_D$.

As reported by DR experiments in Ref. 12, use of the following parameters, $\varepsilon_0 \sim 40 \times 10^6$, $\varepsilon_\infty \sim 20$ and $\tau_D \sim 10$ ms, leads to $\tau_L \sim 50$ ns at ~ 300 K) predicts a solvation time constant (τ_L) of ~ 50 ns for a dipolar probe in these melts at 303 K, should they possess, as reported for (CH_3CONH_2 + NaCNS) melts[12], an extremely large ε_0 ($\sim 10^6$) and a Debye relaxation time (τ_D) of ~ 10 ms. The fact that the solvent reorganization is nearly complete within a couple of nanosecond only suggests that either both the ε_0 and τ_D are much smaller than their projected values, or, their coupling to solvation processes renders undetectably small contribution in the 20 ns time-window employed in the present measurements. Even though the second possibility could be a reason for the non-observation of the predicted extremely slow dynamics, it is difficult to understand why the present experiments would not be able to capture a timescale, if exists, 2–3 times slower than the observed one. Such a slower timescale is expected to originate from the coupling of the millisecond motion of ion-solvent clusters or ion-induced solvent aggregates[3,12,13] to the time-dependent density fluctuations at different wavevectors.[32] In contrast, solvation response functions presented in this figure and other measured ones have been found to fit to bi-exponential functions of time, substantial portion ($0.24 \leq a_1 \leq 0.60$) of which decays with a time constant $32 \leq \tau_1/ps \leq 112$, followed by a slower component (a_2) with a time constant $475 \leq \tau_2/ps \leq 770$. Parameters obtained from bi-exponential fits to the measured decays have been summarized in Table S9 (see supplementary material[84]). Note that these time scales resemble those associated with biphasic solvation observed earlier for one component molten inorganic salts at elevated temperatures.[111]

Next we investigate the possible mechanisms for the observed biphasic solvation in these complex mixtures because motions of both ions and host polar solvent molecules couple to solvation energy relaxation in these non-aqueous electrolyte solutions. As in Ref. 31, both the overdamped and the underdamped dynamics of solvation have been considered. While solvation in the overdamped limit is known to be carried out by the diffusive modes (both rotational and translational) and thus governed entirely by the solution viscosity, underdamped limit accounts also for the contributions from the inertial motions of the particles.[63,110(a)] Method of calculation, discussed in the Supplementary material[84] (A1), illustrates how dielectric relaxation parameters[110(b)] have been approximated in the absence of any experimental data for these mixtures and how these parameters incorporated into the subsequent calculations. We only mention here that the calculated total solvation response functions are composed of 90% contributions from pure polar solvent dynamics and only 10% from ion dynamics, although a small variation in the relative contributions does not affect the qualitative feature of the predicted results. This means the calculated total solvation response function is constructed as, $S_{ss}(t) = 0.9S_{sd}(t) + 0.1S_{si}(t)$, where $S_{sd}(t)$ and $S_{si}(t)$ are given respectively by Eqs. (3a) and (4a) of A1 (see supplementary material[84]). Such an approach has not only provided a successful description of experimental Stokes shift dynamics in neat ionic liquids[59,60] and (ionic liquid + polar solvent) binary mixtures[62(b)] but also explained semi-quantitatively the measured dynamics in a few such molten mixtures.[31,32] Note the above construction of $S_{ss}(t)$ closely follows the observation made earlier in experimental studies of Stokes shift dynamics of polar probe in electrolyte solutions at ambient condition,[112] where ion-dynamics has been found to contribute $\sim 20\%$ to the total dynamics and that too at the later stage of the solvation energy relaxation.

As observed in experiments for these melts, $S_{ss}(t)$, calculated in both the overdamped and the underdamped limits, have been found to be bi-exponential function of time at all compositions and temperatures studied. The fast solvation time constants (τ_1), obtained from the overdamped calculations at three different temperatures, are compared in Fig. 7

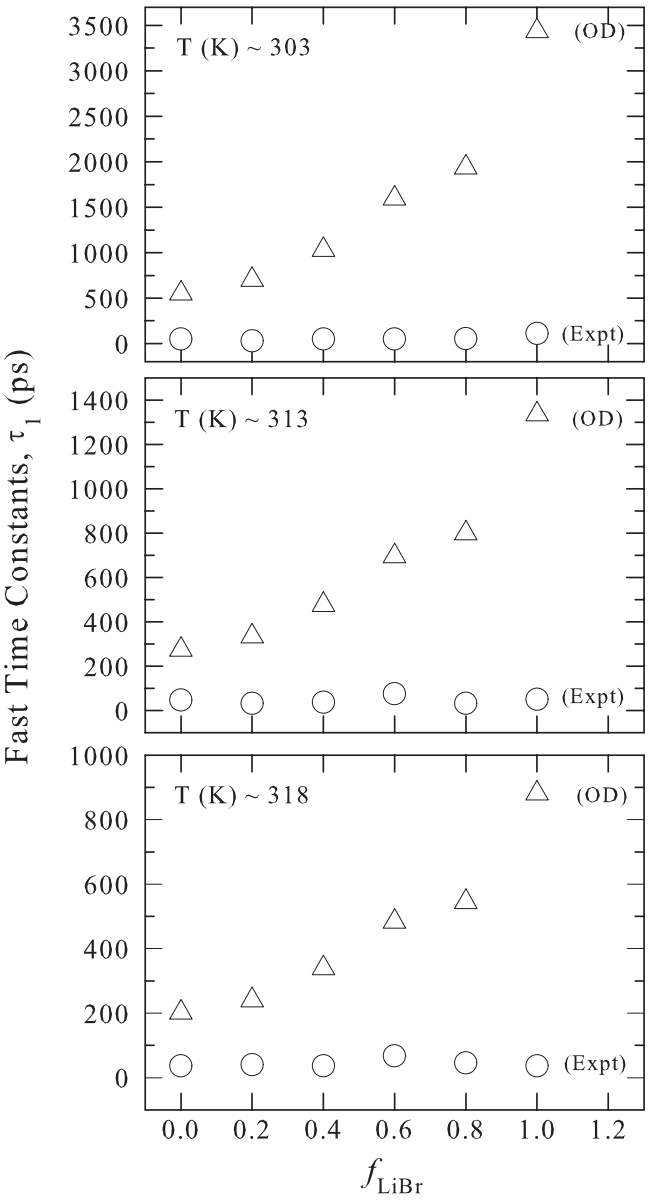

FIG. 7. A comparison between the composition dependent measured fast solvation time constants (circles) and those calculated from our semi-molecular theory (described in A1, supplementary material) in the overdamped limit (triangles) at 303 K (upper panel), 313 K (middle panel), and at 318 K (lower panel). These time constants (τ_1) have been obtained from fitting of the measured and calculated solvation response functions as described in the text. The uncertainty associated with the experimental times is ±5% of the reported values.

with those from experiments. The amplitudes associated with τ_1 are also ~50% (see Table S10, supplementary material[84]) and thus close to experimental data. τ_1 from underdamped calculations have not been shown because they are too short ($0.9 < \tau_1/ps < 3$) to be presented in the same figure although their amplitudes are quite substantial (38–40%). Interestingly, the comparison reveals while the calculated fast time constant (τ_1) increases with LiBr concentration in the melt (which follows LiBr concentration dependence of viscosity), the experimental counter-part remains nearly insensitive. This indicates that either the experimental fast time constant is not entirely controlled by the medium viscosity or a certain degree of decoupling between motions of solvating particles and medium viscosity exists. Participation of underdamped solvent modes (such as amide intermolecular librations[93,94]) is known[63] to reduce the importance of viscosity for the initial fast component of the total polar solvation energy relaxation in liquid solvents. For these multi-component mixtures, this is demonstrated in Fig. 8 where composition dependent calculated slow solvation time constants (τ_2) at three different temperatures have been compared with those from experiments. Better agreement between the underdamped calculations and the experiments for τ_2 only reinforces the notion that much faster timescales than those set by particle diffusion exist in these melts, and significant portion of the polar solvation energy relaxes via the participation of the solvent librational modes. Interestingly, the agreement between the time constants from underdamped calculations and experiments are not as good at 303 K as those at the other two higher temperatures. Like in supercooled liquids, if the heterogeneity is more pronounced at higher medium viscosity, then the molten mixtures at 303 K are expected to be more heterogeneous than at 313 K and 318 K. Consequently, solvation times would be more decoupled from solution viscosity at 303 K, showing poorer agreement between experiments and such simple calculations where heterogeneity has not been considered at all. It should, however, be recognized that overdamped predictions at the highest temperature, even though not as quantitative as those from underdamped calculations, are qualitatively in the same range ($400 < \tau_2(OD)/ps < 3200$) as observed in experiments ($400 < \tau_2(Expt.)/ps < 1000$). Such an observation encourages one to investigate, within the framework of a simplistic model, the density fluctuation length-scales which are probably associated with the solvation time constants (τ_1 and τ_2) measured in the present experiments.

Figure 9 shows the mixture composition dependent structural relaxation times corresponding to medium density fluctuations at the collective ($k\sigma \sim 0$) and nearest-neighbor ($k\sigma \sim 2\pi$) wavevectors, calculated in the overdamped limit at 318 K where the heterogeneity is supposed to be the minimum. While the upper panel depicts the composition dependence of the orientational structural relaxation time (τ_{str}^{rot}), the time constants associated with the relaxation of the ion dynamic structure factor (τ_{str}^{trans}) are presented in the lower panel. Note that τ_{str}^{rot} and τ_{str}^{trans} have been calculated respectively by using equations (6) and (15) described in A1 (see supplementary material[84]). Data in Fig. 9 suggest that the fast timescale measured in the present experiments ($32 \leq \tau_1/ps \leq 112$) originates from the diffusive ion density

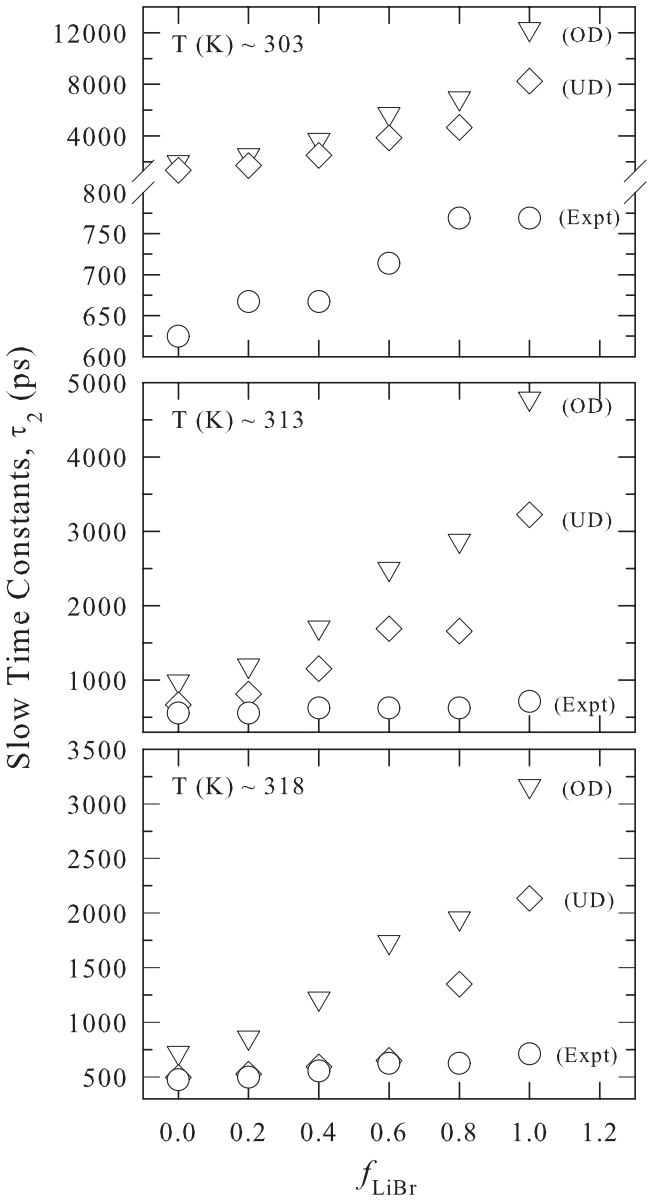

FIG. 8. Similar comparison as in Fig. 7 but for the slower solvation time constants (τ_2) obtained from measurements (circles) and from calculations in the overdamped limit (inverted triangles) and underdamped limit (diamonds) at three different temperatures for C153 in these melts at different compositions. Uncertainty in measured τ_2 remains the same as for measured τ_1.

fluctuations at $k\sigma \sim 2\pi$ modes, whereas the slow ones ($400 < \tau_2/ps < 1000$) are associated with the orientational density fluctuations of the polar solvent involving both the collective ($k\sigma \sim 0$) and the nearest neighbor ($k\sigma \sim 2\pi$) modes. These results in conjunction with the underdamped prediction of ~50% solvation energy relaxation with time constants in ~1–3 ps range, and missing of a substantial portion (~20–50%) of the dynamics by the present experiments clearly indicate the domination of the orientational solvent density fluctuations involving the collective modes. In addition, the predicted near insensitivity of fast time constant ($0.9 < \tau_1/ps < 3$) on f_{LiBr} in the underdamped limit is in accordance with the general results from simulation studies[113–115] of solvation dynamics in electrolyte solutions. Note that similar fast timescale has also been predicted earlier for (acetamide

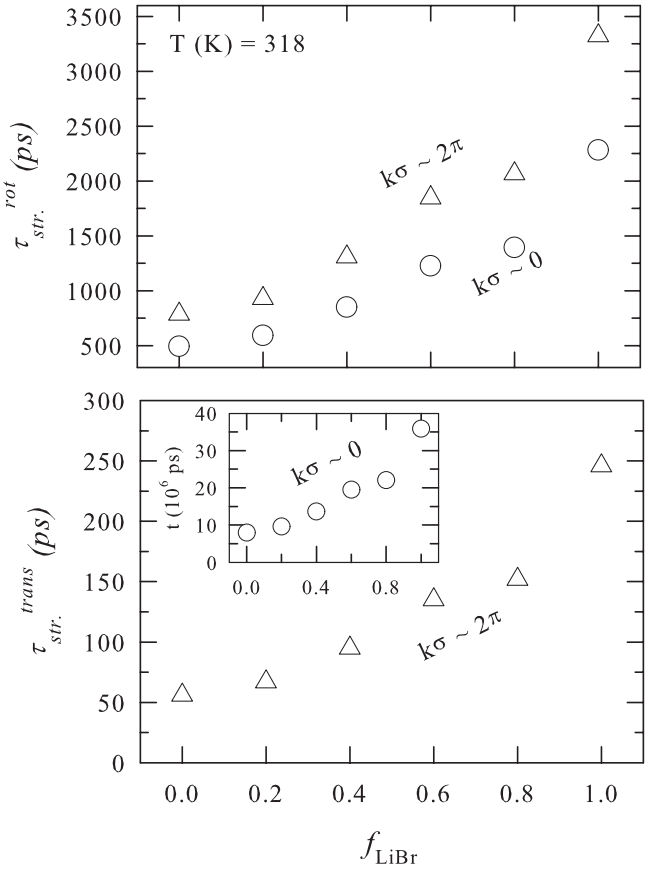

FIG. 9. Origin of the fast and slow solvation timescales as predicted by the semi-molecular theory for these molten mixtures at different compositions. Timescales arising from density fluctuations at relevant wavenumber modes are specified in each of the panels. Expressions for τ_{str}^{rot} and τ_{str}^{trans} are provided in the supplementary material (A1).

+ sodium/potassium thiocyanate)[31] and (acetamide + calcium nitrate)[32] molten mixtures. *Inset* (lower panel) shows the timescale associated with the collective ($k\sigma \sim 0$) ion density fluctuations, which is extremely slow and has not been observed in our experiments. This seems to suggest that either the collective ion density fluctuations are irrelevant for polar solvation energy relaxation in these melts or their contribution is too small to be detected by the present experimental set-up.

C. Stokes shift dynamics: Decoupling from medium viscosity

Next we illustrate the coupling between average solvation time ($\langle\tau_s\rangle$) and medium viscosity (η) in Fig. 10 where, in a log-log plot, the composition dependent $\langle\tau_s\rangle$ measured for these melts at 303 K, 313 K, and 318 K are shown as a function of temperature-reduced viscosity, η/T. Since $\langle\tau_s\rangle$ is dominated by the spatial diffusion timescale of medium particles (τ_2 in these cases) and since the Stokes-Einstein (SE) relation predicts, $D^{-1}\infty(\eta/T)$ (D being diffusion coefficient), such a plot is expected to reflect on the validity of the SE relation in these melts. Fig. 10, however, exhibits a power-law dependence on reduced viscosity, $\langle\tau_s\rangle \infty (\eta/T)^p$, with an average value for the power ($p = 0.35$) much less than unity. Treatment of $\langle\tau_s\rangle$ as separate sets (see Fig. S11, supplementary material[84]) produces slightly different values for p: 0.34 at 303 K, 0.32 at 313 K and 0.40 at 318 K. Our attempt to fit to the form, $\langle\tau_s\rangle \infty \eta^p$, also produces equally good description with p values nearly the same as above. These analyses confirm presence of pronounced heterogeneity in these molten mixtures, the extent being the larger at lower temperature, providing an experimental support to the logic used earlier while explaining the relatively poorer agreement between predicted and measured slower solvation time constants at 303 K (see Fig. 8). Note the pronounced fractional viscosity dependence of $\langle\tau_s\rangle$ is quite reminiscent of viscosity-decoupling of diffusion in deeply supercooled liquids, and may therefore indicate presence of both static (distribution of environments) and dynamic heterogeneities (distribution of relaxation times)[35–41] in these molten mixtures. Surprisingly, dynamic Stokes shift measurements in ionic liquids, systems which are somewhat similar to these multi-component mixtures both in interaction and heterogeneity aspects, do not show fractional SE behavior,[66] even though such a fractional viscosity dependence has been experimentally observed for ion transport in ionic melts.[116] In addition, significant departure from the conventional SE relation is also expected for diffusion of small solutes in a medium of large particles.[117] Therefore, non-hydrodynamic diffusion of lighter alkali metal ions- Li^+ for the present melts and Na^+/K^+ for other molten mixtures[31] might be one of the reasons for the observed fractional viscosity dependence of $\langle\tau_s\rangle$.

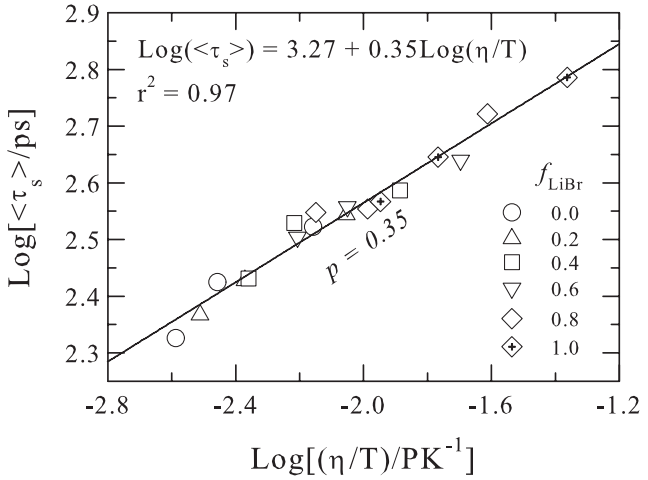

FIG. 10. Log-log plot of average solvation time, $\langle\tau_s\rangle$ of C153 versus η/T in molten mixtures of acetamide with lithium nitrate and lithium bromide. The solid line shows the best fit of the experimentally measured data to the relation $\text{Log}[\langle\tau_s\rangle] = \text{B} + p\text{Log}[\eta/\text{T}]$, the associated B and p value are given in the figure. Different symbols represent data at different mixture compositions.

D. Dynamic fluorescence anisotropy measurements: Heterogeneity and medium decoupling

Representative fluorescence anisotropy decays of C153 at different temperatures and compositions are presented in Fig. 11 in order to show the effects on $r(t)$ of temperature (upper panel) and Br^- ion concentration (lower panel). Both the effects of temperature on $r(t)$ at a given composition and that of LiBr concentration at a fixed temperature can be explained

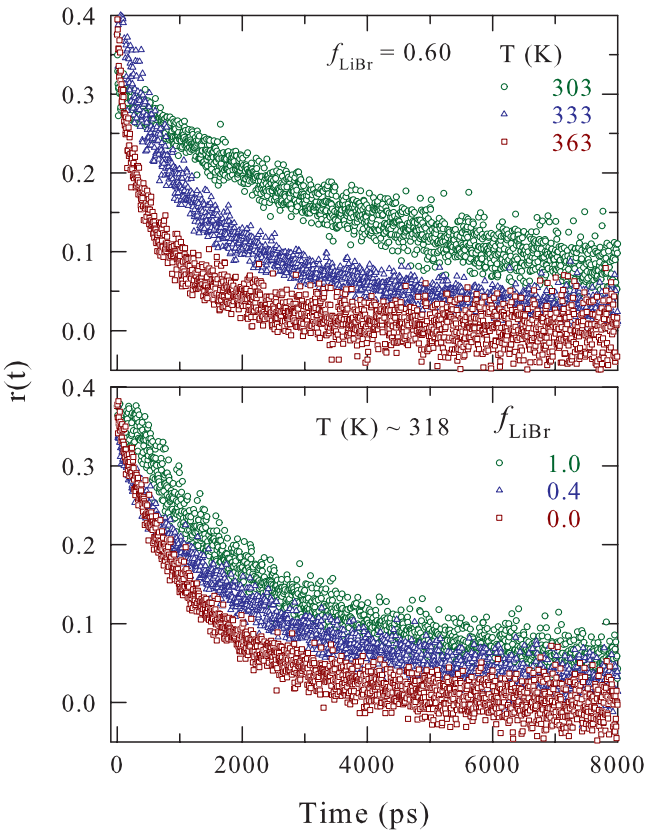

FIG. 11. Temperature and composition effects on fluorescence anisotropy ($r(t)$) decay of C153 in [0.78CH_3CONH_2 + 0.22{f LiBr + (1-f) $LiNO_3$)] molten mixtures. Data representations are clearly explained inside the panels.

by the temperature and composition dependence of viscosity of these melts (see Table S8, supplementary material[84]). As already mentioned, $r(t)$ decays, collected at various temperatures and mixture compositions, can be adequately described by a sum of two exponentials. A representative fit is provided in the supplementary material[84] (Fig. S12) along with the residual, which shows the general quality of the unconstrained bi-exponential fits to the experimental $r(t)$ decays. Fit parameters summarized in Table S13 (see supplementary material[84]) demonstrate that these biphasic anisotropy decays are characterized by a substantial (~30–65%) fast amplitude with time constant in ~10–30 ps range, and a very slow component with time constant spreading between ~0.7 ns and ~12 ns. The fast time constants are therefore too short to be accurately detected by the present experiments and hence any particular dependence of them on Br^- concentration or temperature cannot be explored. Also note that missing of these fast components might have led to the observation of bi-exponential dynamics in place of stretched exponential ones expected for these heterogeneous molten mixtures.[118]

The slow time constant, on the other hand, decreases with temperature at a given composition and increases with Br^- concentration at a given temperature. These are in accordance with the hydrodynamic prediction because we find viscosity at a fixed composition reduces upon increasing temperature and increases with Br^- concentration (at a given temperature). Effects of temperature and composition on C153 rotation in these melts are more clearly depicted in Fig. S14 (see supplementary material[84]) where the average rotation and solvation times ($\langle\tau_r\rangle$ and $\langle\tau_s\rangle$, respectively), and experimental viscosities from our independent isocomposition and isothermal measurements are shown as a function of f_{LiBr} for different temperatures. Note both $\langle\tau_s\rangle$ and $\langle\tau_r\rangle$ increase with viscosity and decrease with temperature, suggesting a dominant role for the medium viscosity in controlling the average rates for the time-dependent solvation and fluorescence anisotropy in these melts. However, this does not rule out the possibility of complexation between C153 and ions present in the melt, as found during the study of rotational relaxation of resorufin in electrolyte solutions,[119] contributing to the measured $\langle\tau_r\rangle$. Note that the slow rotation time constants at high Br^- concentrations (particularly those at 303 K) are ~2–3 times larger than the excited state lifetime (~5 ns) of C153. Such a longer time constant for these melts is not improbable because in ionic liquids near room temperature rotational time constants for solutes larger by a factor of ~2–20 than their respective excited state lifetimes have been reported and explained in terms of heterogeneous solution structure.[66,120–122] However, this does not anyway confirm that the observed biphasic behavior of $r(t)$ originates exclusively from solutes trapped in different solvent environments but rather suggests that both the non-Markovian nature of the underlying friction and solution structural heterogeneity could be responsible for the biphasic character of the measured anisotropy decays.[80]

Next the appropriateness of the Stokes-Einstein-Debye (SED) relation in describing the solute rotational diffusion in these melts is explored in Fig. 12 where the measured $\langle\tau_r\rangle$ at all compositions and temperatures have been shown as a function of temperature-reduced viscosity, η/T. Note the data are shown in a log-log plot. The corresponding SED values have been calculated by using the formula, $\langle\tau_r\rangle = \frac{V\eta}{k_BT} fC$, with solute volume $V = 246$ Å^3, shape factor $f = 1.71$, and solute-solvent coupling parameter $C = 0.24$ (for slip boundary condition) and 1.0 (for stick boundary condition).[66] A comparison with the SED predictions indicates that, at higher

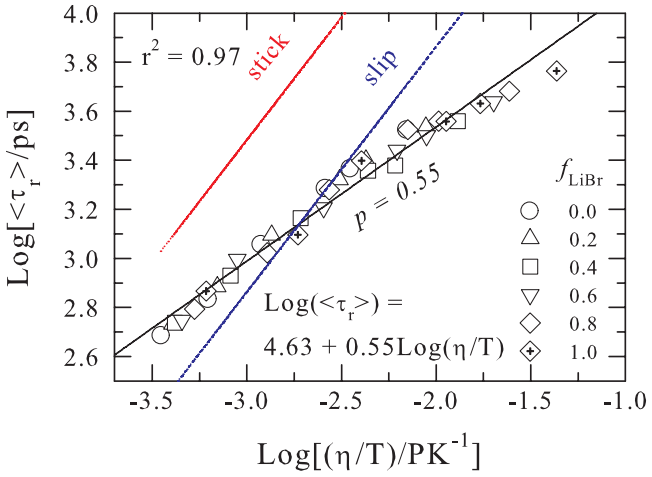

FIG. 12. Log-log plot of average rotation time, $\langle\tau_r\rangle$ of C153 versus η/T in molten mixtures of acetamide with lithium nitrate and lithium bromide. The solid line shows the best fit of the experimentally measured data to the relation Log[$\langle\tau_r\rangle$] = B + pLog[η/T], the associated B and p value are given in the figure. The dashed lines show the prediction of hydrodynamic stick and slip limits. Different symbols denote data at different mixture compositions.

temperatures (in low η/T limit), measured $\langle\tau_r\rangle$ lies between the slip and stick predictions but becomes sub-slip in the large η/T limit at low temperature. The departure from the SED predictions is quantified as, $\langle\tau_r\rangle \propto (\eta/T)^p$, with an average $p = 0.55$. This can be explained by considering that shorter heterogeneity lifetime at higher temperatures allows better environmental averaging of the relaxation dynamics, leading to a more hydrodynamic behavior.[123] At lower temperatures where heterogeneities are longer-lived than $\langle\tau_r\rangle$, molecular aspects get prominence and a departure from the SED description ensues. Results obtained from experimental studies of reactive and non-reactive dynamics in ionic liquids,[52,124,125] and those from very recent measurements after isothermal introduction of ~2 nm structural inhomogeneity in an otherwise homogeneous liquid[126] suggest that both the static and dynamic heterogeneities could contribute to the observed decoupling between solute rotation and viscosity in these melts. In the absence of $LiNO_3$ ($f_{LiBr} = 1.0$) the extent of decoupling becomes even stronger as one finds $p = 0.50$ at this composition (see Fig. S15, supplementary material[84]). This is expected as larger viscosity in an inhomogeneous medium is known to produce larger decoupling.[35] The deviation at the high η/T regime is likely to originate from non-Brownian moves, such as large angle jumps[127] and retention of inertia-driven motion even much after the onset of the typical diffusion timescale.[128,129] These alternative dynamic modes significantly reduce the frictional resistance against the diffusing particle arising from the macroscopic viscosity and thus strongly promotes departure from the conventional hydrodynamic description. Note that complexation through an interaction between the π-electron system and halide, particularly for compounds with electron-deficient aromatic ring, is a well-known phenomenon[130,131] and therefore formation of C153-Br^- complex in presence of LiBr in these melts may also modify the expected hydrodynamic behavior of the solute rotation.

Even though the viscosity dependence of $\langle\tau_r\rangle$ in these melts at different compositions could be represented in Fig. 12 by $\langle\tau_r\rangle \propto (\eta/T)^p$ with an *average* value of p, there exists a subtle composition dependence for p. This is depicted in Fig. 13 where p obtained from fits of the measured $\langle\tau_r\rangle$ to both the medium viscosity ($\langle\tau_r\rangle \propto \eta^p$) and the temperature-reduced viscosity ($\langle\tau_r\rangle \propto (\eta/T)^p$) are shown as a function of the mixture composition, f_{LiBr}. Figure 13 clearly shows that the composition dependent p values obtained from both fits are not very different from each other, indicating that the temperature dependence of $\langle\tau_r\rangle$ is essentially that of the medium viscosity, η. Interestingly, these data indicate LiBr-rich region is more heterogeneous than the $LiNO_3$ enriched melt, an observation is contrary to the steady state measurements shown in Fig. 3. Although this heterogeneity character (as revealed by the present anisotropy measurements using C153) is expected on viscosity consideration, is opposite to the trend reported for the η-α relationship (α being the stretching exponent required to numerically fit the measured DR spectra) explored via DR experiments for several alkylimidazolium aluminate ionic liquids.[132] All these experimental results therefore indicate more extensive studies to explore the molecular origin for viscosity decoupling of dynamical variables in complex systems where electrostatic interactions play a significant or dominant role.

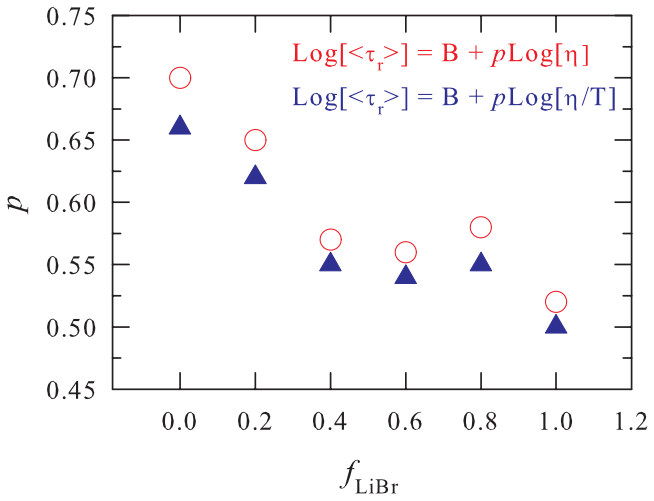

FIG. 13. Composition (f_{LiBr}) dependence of p, obtained from fitting the measured $\langle\tau_r\rangle$ in these molten mixtures to the following expressions: Log[$\langle\tau_r\rangle$] = B + pLog[η/T] (triangles), and Log[$\langle\tau_r\rangle$] = B + pLog[η] (circles). Note that both fits produce comparable p values and quite smaller than unity.

Since the temperature dependence of viscosity of these melts shows a weak deviation from the linearity in Arrhenius description (that is, ln η vs. $1/T$ plot), one can extract activation energies from the measured average times ($\langle\tau_r\rangle$ and $\langle\tau_s\rangle$) and correlate their ratio with that between fraction powers (p) associated with the probe solvation and rotation. If the small nonlinearity is neglected and the temperature dependence of viscosity is approximated to be Arrhenius-type, one obtains the following general expression for the temperature dependence of average rates (solvation and rotation), $\ln(1/\langle\tau_x\rangle) = C - E_a^x/RT$, where E_a^x denote the activation energy obtained from either average solvation times ($\langle\tau_s\rangle$) or from average rotation times ($\langle\tau_r\rangle$). This is related to the viscosity activation energy (E_a) as follows: Assume $\eta = \eta_0 \exp(E_a/RT)$ and recall that the measured average times have shown the following viscosity dependence: $\langle\tau_x\rangle = A_x\eta^p$, x denoting solvation (s) or rotation (r). Insertion of the above Arrhenius description of temperature dependent η into the expression of $\langle\tau_x\rangle$ leads to $\ln(1/\langle\tau_x\rangle) = C - E_a^x/RT$, where $E_a^x = pE_a$. Therefore, $E_a^r/E_a^s = p^r/p^s$, where p^x is the fractional power obtained from the viscosity dependence of average rotation or solvation times): $E_a^x = p^x E_a$. Fig. S16 (see supplementary material[84]) indicates ln $(1/\langle\tau_x\rangle)$ vs. $1/T$ plots are approximately linear for these melts, and therefore activation energies at various compositions of the melt can be obtained from the respective slopes. Activation energies (E_a^x) thus obtained are presented in Fig. 14 where E_a^x from both the measured average solvation and rotation times are shown as a function of LiBr concentration, f_{LiBr}. Note that activation energies obtained from $\langle\tau_r\rangle$ are, on an average, 1.5 times larger than those obtained from $\langle\tau_s\rangle$. This is expected because in these melts the extent of coupling to medium viscosity is approximately 1.5 times stronger for solute rotation than that for solute solvation (see Table S16, supplementary material[84]). Composition dependent p values summarized in

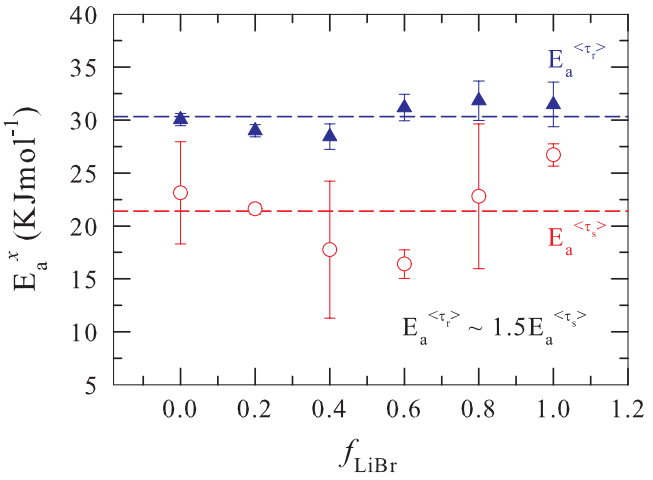

FIG. 14. Activation energies (E_a^x) obtained from the measured average solvation and rotation times ($\langle\tau_s\rangle$ and $\langle\tau_r\rangle$ respectively). Note the ratio between activation energies at any composition closely follows that between p values.

this table also reveal that solute-solvent interaction in these melts does not alter much even for moving from one binary end to the other. This is the reason for near-insensitivity of both $E_a^{\langle\tau_r\rangle}$ and $E_a^{\langle\tau_s\rangle}$ on mixture composition shown in Fig. 14. Estimation of composition dependent activation energies using our earlier rotation data for C153 in [0.75CH_3CONH_2 + 0.25{f KSCN + (1-f) NaSCN)] melts[31] have produced ~40 KJmol^{-1} and 35 KJmol^{-1} as $E_a^{\langle\tau_r\rangle}$, respectively, for $f_{KSCN} = 0.2$ and $f_{KSCN} = 0.8$, which are very close to what have been observed in the present [0.78CH_3CONH_2 + 0.22{f LiBr + (1-f) $LiNO_3$)] molten mixtures. Interestingly, average activation energies obtained from $\langle\tau_r\rangle$ in both these melts are quite close to that determined from viscoelastic measurements of (CH_3CONH_2 + CF_3COONa) binary melt at the highest salt concentration.[3] This similarity perhaps indicates near-equivalence in modifications of solution structure and dynamics by different alkali metal salts in molten acetamide.

IV. CONCLUSION

In summary, the fluorescence spectroscopic results presented here indicate pronounced solution heterogeneity in molten mixtures of acetamide with lithium nitrate and bromide, the extent of which is perhaps even stronger than that in molten mixtures of acetamide with sodium and potassium thiocyanates. Particularly interesting in this mixture is the anisotropy sensing of stronger heterogeneity in Br^- dominated region which is anti-correlated with the steady state fluorescence results from excitation wavelength dependence study. Breakdown for both the SE and DSE relations along with strong decoupling between solute diffusion and medium viscosity have been observed. Quite reminiscent of the behavior of transport properties in deeply supercooled neat liquids, a strong decoupling between translation and rotation in these melts has also been demonstrated. These results have been explained in terms of both static and dynamic heterogeneities even though quantitative measurements of neither spatial nor temporal heterogeneities have been made in the present work. Measured Stokes shift dynamics and application of a semi-molecular theory suggest presence of a significant sub-picosecond solvation response in these highly viscous melts. This theory also indicates that the measured solvation timescales originate from the orientational polarization density relaxations involving both the collective and nearest neighbor solvent modes, and the isotropic structural relaxation involving only the nearest neighbor modes. Remarkably, consideration of fluorescence spectroscopic (both steady state and time-resolved) results together with the theoretical predictions does not support the idea of colossal dielectric constant and extremely slow relaxation timescale in these melts.

Since the heterogeneity character of these melts could not be quantified, the present study should motivate small angle neutron scattering (SANS) and X-ray scattering (SAXS) measurements so that the length-scales over which the particles are correlated are revealed. Excitation wavelength dependent measurements of solute rotation and solvation, on the other hand, will be useful in understanding the temporal heterogeneity in these complex systems. The applicability of the fractional single-file diffusion model[133,134] in explaining the observed breakdown of the SE and SED relations could be investigated. Our recent model simulation studies with a similar melt have indicated presence of strong dynamic heterogeneity and cooperative blockage in ion motions.[135] An atomistic simulation studies should therefore be carried out to quantify the roles of both static and dynamic heterogeneities in determining the viscosity decoupling observed in these melts. It would also be interesting as well as challenging to connect the particle jump, anisotropic local stress relaxation, and the leading density modes to the observed decoupling.[136–138] While stating these it should be kept in mind that the breakdown of SE and SED relations can occur for a variety of reasons. For example, several theories have indicated that the mechanism for breaking down of these hydrodynamic relations for high temperature melts could very well be different from that causing the break-down of SE relation near $1.2T_g$ in structural glass formers.[139,140] Indeed, the break-down is expected for molecular systems because these hydrodynamic relations were developed for macroscopic particles moving in a continuum field. Therefore, further studies involving experiments, atomistic simulations and analytical theories would be required to fully understand these complex molten systems.

ACKNOWLEDGMENTS

We acknowledge the help received from Dr. T. Pradhan and Dr. H. K. Kashyap in accessing many important references cited here. We thank the anonymous reviewers for constructive criticisms. B.G. and S.D. acknowledge the Council of Scientific and Industrial Research (CSIR), India for providing them with research fellowships. R.B. thanks Professor H. Shirota, Chiba University, Japan for excellent hospitality.

[1] M. Gusteri, V. Bartocci, F. Castellani, and F. Pucciarelli, J. Electroanal. Chem. **102**, 199 (1979).
[2] F. Castellani, G. Berchiesi, F. Pucciarelli, and V. Bartocci, J. Chem. Eng. Data **26**, 150 (1981).
[3] G. Berchiesi, M. D. Angelis, G. Rafaiani, and G. Vitali, J. Mol. Liq. **51**, 11 (1992).

[4]F. Castellani, G. Berchiesi, F. Pucciarelli, and V. Bartocci, J. Chem. Eng. Data **27**, 45 (1982).
[5]G. Berchiesi, G. G. Lobbia, V. Bartocci, and G. Vitali, Thermochim. Acta **70**, 317 (1983).
[6]G. G. Lobbia, G. Berchiesi, and G. Poeti, Thermochim. Acta **74**, 247 (1984).
[7]G. Berchiesi, G. G. Lobbia, M. A. Berchiesi, and G. Vitali, J. Therm. Anal. **29**, 729 (1984).
[8]G. G. Lobbia and G. Berchiesi, Thermochim. Acta **74**, 251 (1984).
[9]G. G. Lobbia and G. Berchiesi, Thermochim. Acta **72**, 391 (1984).
[10]G. Berchiesi, G. Rafaiani, G. Vitali, and F. Farhat, J. Therm. Anal. **44**, 1313 (1995).
[11]G. Berchiesi, G. Vitali, P. Passamonti, and R. Plowiec, J. Chem. Soc. Faraday Trans. 2 **79**, 1257 (1983).
[12]A. Amico, G. Berchiesi, C. Cametti, and A. D. Biasio, J. Chem. Soc. Faraday Trans. 2 **83**, 619 (1987).
[13]G. Berchiesi, J. Mol. Liq. **83**, 271 (1999).
[14]O. F. Stafford, J. Am. Chem. Soc. **55**, 3987 (1933).
[15]L. F. Yntema and L. F. Audrieth, J. Am. Chem. Soc. **52**, 2693 (1930).
[16]L. R. Dawson, P. G. Sears, and R. H. Graves, J. Am. Chem. Soc. **77**, 1986 (1955).
[17]R. A. Wallace, Inorg. Chem. **11**, 414 (1972).
[18]R. Wallace, J. Phys. Chem. **75**, 2687 (1971).
[19]D. H. Kerridge, Chem. Soc. Rev. **17**, 181 (1988).
[20]G. Jander and G. Winkler, J. Inorg. Nucl. Chem. **9**, 24 (1959).
[21]R. Wallace and P. J. Bruins, Electrochem. Soc. **114**, 212 (1967).
[22]G. E. McManis, A. N. Fletcher, D. E. Bliss, and M. H. Miles, J. Electroanal. Chem. **190**, 171 (1985).
[23]G. Kalita, K. G. Sarma, and S. Mahiuddin, J. Chem. Eng. Data, **44**, 222 (1999).
[24]G. Kalita, N. Rohman, and S. Mahiuddin, J. Chem. Eng. Data **43**, 148 (1998).
[25]S. Mahiuddin, J. Chem. Eng. Data **41**, 231 (1996).
[26]G. Berchiesi, F. Farhat, and M. D. Angelis, J. Mol. Liq. **54**, 103 (1992).
[27]G. Berchiesi, G. Vitali, R. Plowiec, and S. Barocci, J. Chem. Soc. Faraday Trans. 2 **85**, 635 (1989).
[28]K. S. Cole and R. H. Cole, J. Chem. Phys. **9**, 341 (1949).
[29]D. W. Davidson and R. H. Cole, J. Chem. Phys. **19**, 1484 (1951).
[30]P. Debye, *Polar Molecules* (Chemical Catalogue Company, New York, 1929).
[31]B. Guchhait, H. A. R. Gazi, H. Kashyap, and R. Biswas, J. Phys. Chem. B **114**, 5066 (2010).
[32]H. A. R. Gazi, B. Guchhait, S. Daschakraborty, and R. Biswas, Chem. Phys. Lett. **501**, 358 (2011).
[33]P. W. Atkins, *Physical Chemistry*, 5th ed. (Oxford University Press, Oxford, 1994).
[34]J. R. Lakowicz, *Principles of Fluorescence Spectroscopy*, 2nd ed. (Kluwer Academic, New York, 1999).
[35]M. D. Ediger, Annu. Rev. Phys. Chem. **51**, 99 (2000).
[36]H. J. Sillescu, Non-Cryst. Solids **243**, 81 (1999).
[37]M. D. Ediger, C. A. Angell, and S. R. Nagel, J. Phys. Chem. **100**, 13200 (1996).
[38]I. Chang, F. Fujara, B. Geil, G. Heuberger, T. Mangel, and H. Sillescu, J. Non-Cryst. Solids **172–174**, 248 (1994).
[39]C. T. Moynihan, J. Phys. Chem. **70**, 3399 (1966).
[40]C. A. Angell, J. Chem. Phys. **46**, 4673 (1967).
[41]D. Chakrabarti and B. Bagchi, Phys. Rev. Lett. **96**, 187801 (2006).
[42]C. G. Gray and K. E. Gubbins, *Theory of Molecular Fluids* (Clarendon, Oxford, 1984), Vol. I; P. A. Egelstaff, *An Introduction to the Liquid State* (Clarendon, Oxford, 1992); J. P. Hansen and I. R. McDonald, *Theory of Simple Liquids* (Academic, London, 1986).
[43]E. W. Castner, Jr., C. J. Margulis, M. Maroncelli, and J. F. Wishart, Annu. Rev. Phys. Chem. **62**, 85 (2011).
[44]Y. Wang and G. A. Voth, J. Am. Chem. Soc. **127**, 12192 (2005); J. Phys. Chem. B **110**, 18601 (2006).
[45]B. L. Bhargava, M. L. Klein, and S. Balasubramanian, ChemPhysChem **9**, 67 (2008); B. L. Bhargava, R. Devane, M. Klein, and S. Balasubramanian, Soft Matter **3**, 1395 (2007); S. G. Raju and S. Balasubramanian, J. Phys. Chem. B **114**, 6455 (2010).
[46]J. A. C. Lopes and A. A. H. Padua, J. Phys. Chem. B **110**, 3330 (2006).
[47]S. M. Urahata and M. C. C. Ribeiro, J. Chem. Phys. **120**, 1855 (2004).
[48]J. D. Andrade, E. S. Boes, and H. Stassen, J. Phys. Chem. B **112**, 8966 (2008); **113**, 7541 (2009).
[49]A. Triolo, O. Russina, H. Bleif, and E. D. Cola, J. Phys. Chem. B **111**, 4641 (2007); A. Triolo, O. Russina, B. Fazio, G. B. Appetecchi, M. Carewska, and S. Passerini, J. Chem. Phys. **130**, 164521 (2009); A. Triolo, O. Russina, B. Fazio, R. Triolo, and E. D. Cola, Chem. Phys. Lett. **467**, 362 (2008).
[50]W. Zheng, A. Mohammed, L. G. Hines, D. Xiao, O. J. Martinez, R. A. Bartsch, S. L. Simon, O. Russina, A. Triolo, and E. L. Quitevis, J. Phys. Chem. B **115**, 6572 (2011); D. Xiao, J. R. Rajian, S. Li, R. Bartsch, and E. L. Quitevis, *ibid.* **110**, 16174 (2006); D. Xiao, J. R. Rajian, A. Cady, S. Li, R. Bartsch, and E. L. Quitevis, *ibid.* **111**, 4669 (2007); D. Xiao, L. G. Hines, Jr., R. A. Bartsch, and E. L. Quitevis, *ibid.* **113**, 4544 (2009); D. Xiao, J. R. Rajian, L. G. Hines, Jr., S. Li, R. A. Bartsch, and E. L. Quitevis, *ibid.* **112**, 13316 (2008); D. Xiao, L. G. Hines, Jr., S. Li, R. A. Bartsch, E. L. Quitevis, O. Russina, and A. Triolo, *ibid.* **113**, 6426 (2009); O. Russina, A. Triolo, L. Gontrani, R. Caminti, D. Xiao, L. G. Hines, Jr., R. A. Bartsch, E. L. Quitevis, N. Plechkova, and K. R. Seddon, J. Phys.: Condens. Matter **21**, 424121 (2009).
[51]P. K. Mandal, M. Sarkar, and A. Samanta, J. Phys. Chem. A **108**, 9048 (2004).
[52]H. Jin, X. Li, and M. Maroncelli, J. Phys. Chem. B **111**, 13473 (2007).
[53]A. Adhikari, A. K. Sahu, S. Dey, S. Ghose, U. Mandal, and K. Bhattacharyya, J. Phys. Chem. B **111**, 12809 (2007); D. K. Sasmal, A. K. Mandal, T. Mondal, and K. Bhattacharyya, *ibid.* **115**, 7781 (2011).
[54](a) Z. Hu and C. J. Margulis, Proc. Natl. Acad. Sci. U.S.A. **103**, 831 (2006); (b) H. V. R. Annapureddy, H. K. Kashyap, P. M. De Biasse, and C. J. Margulis, J. Phys. Chem. B **114**, 16838 (2010).
[55]D. A. Turton, J. Hunger, A. Stoppa, G. Hefter, A. Thoman, M. Walther, R. Buchner, and K. Wynne, J. Am. Chem. Soc. **131**, 11140 (2009); J. Hunger, A. Stoppa, S. Schrodle, G. Hefter, and R. Buchner, Chem. Phys. Chem. **10**, 723 (2009); A. Stoppa, A. Hunger, R. Buchner, G. Hefter, A. Thoman, and H. Helm, J. Phys. Chem. B **112**, 4854 (2008).
[56]B. Aoun, A. Goldbach, M. A. Gonzalez, S. Kohara, D. L. Price, M.-L. Saboungi, J. Chem. Phys. **134**, 104509 (2011); B. Aoun, A. Goldbach, S. Kohara, J.-F. Wax, M. A. Gonzalez, and M.-L. Saboungi, J. Phys. Chem. B **114**, 12623 (2010); B. Aoun, M. A. Gonzalez, J. Olivier, M. Russina, Z. Izaola, D. L. Price, and M.-L. Saboungi, J. Phys. Chem. Lett. **1**, 2503 (2010).
[57]C. Hardacre, J. D. Holbrey, C. L. Mullan, T. G. A. Youngs, and D. T. Bowron, J. Chem. Phys. **133**, 074510 (2010).
[58]H. K. Kashyap and R. Biswas, J. Phys. Chem. B **112**, 12431 (2008).
[59]H. K. Kashyap and R. Biswas, J. Phys. Chem. B **114**, 16811 (2010).
[60]H. K. Kashyap and R. Biswas, J. Phys. Chem. B **114**, 254 (2010).
[61]H. K. Kashyap and R. Biswas, Ind. J. Chem. **49A**, 685 (2010).
[62](a) S. Daschakraborty and R. Biswas, Chem. Phys. Lett. **510**, 202 (2011); (b) S. Daschakraborty and R. Biswas, J. Phys. Chem. B **115**, 4011 (2011).
[63]B. Bagchi and R. Biswas, Adv. Chem. Phys. **109**, 207 (1999).
[64]R. Biswas and B. Bagchi, J. Phys. Chem. **100**, 4261 (1996).
[65]R. Biswas, N. Nandi, and B. Bagchi, J. Phys. Chem. B **101**, 2968 (1997).
[66]H. Jin, G. A. Baker, S. Arzhantsev, J. Dong, and M. Maroncelli, J. Phys. Chem. B **111**, 7291 (2007).
[67]A. Chandra and S. Chandra, J. Phys. D: Apply. Phys. **27**, 2171 (1994).
[68]B.-K. Choi and Y.-K. Kim, Mat. Res. Soc. Symp. Proc. **369**, 535 (1995).
[69]G. Kalita, N. N. Dass, and S. Mahiuddin, Can. J. Chem. **76**, 1836 (1998).
[70]D. E. Day, J. Non-Cryst. Solids **21**, 343 (1976).
[71]C. T. Moynihan, J. Electrochem. Soc. **126**, 2144 (1979).
[72]A. H. Dietzel, Phys. Chem. Glasses **24**, 172 (1983); M. D. Ingram, *ibid.* **28**, 215 (1987).
[73]H. Vogel, Phys. Z. **22**, 645 (1921); G. S. Fulcher, J. Am. Ceram. Soc. **8**, 339 (1923); G. Tammann and W. Z. Hesse, Anorg. Allgem. Chem. **156**, 245 (1926); C. A. Angell, Chem. Rev. **102**, 2627 (2002).
[74]S. K. Saha, P. Purkayastha, A. B. Das, and S. Dhara, J. Photochem. Photobiol. A: Chem. **199**, 179 (2008); S. K. Saha, P. Purkayastha, A. B. Das, *ibid.* **195**, 368 (2008).
[75]DMASBT was received as a gift from Prof. M. Maroncelli, Penn. State University, USA.
[76]M. L. Horng, J. A. Gardecki, A. Papazyan, and M. Maroncelli, J. Phys. Chem. **99**, 17311 (1995).
[77]C. F. Chapman, R. S. Fee, and M. Maroncelli, J. Phys. Chem. **99**, 4811 (1995).
[78]T. Pradhan and R. Biswas, J. Phys. Chem. A **111**, 11514 (2007).
[79]N. Sarma, J. M. Borah, S. Mahiuddin, H. A. R. Gazi, B. Guchhait, and R. Biswas, J. Phys. Chem. B **115**, 9040 (2011).

[80]M. L. Horng, J. A. Gardecki, and M. Maroncelli, J. Phys. Chem. A **101**, 1030 (1997).
[81]R. Biswas, A. R. Das, T. Pradhan, D. Touraud, W. Kunz, and S. Mahiuddin, J. Phys. Chem. B **112**, 6620 (2008); T. Pradhan, P. Ghoshal, and R. Biswas, J. Chem. Sci. **120**, 275 (2008).
[82]A. J. Cross and G. R. Fleming, Biophys. J. **46**, 45 (1984).
[83]J. A. Riddick, W. B. Bunger, and T. K. Sakano, *Organic Solvents* (Wiley, New York, 1986).
[84]See supplementary material at http://dx.doi.org/10.1063/1.4705315 for steady state and time-resolved data regarding solute solvation and rotation, fit parameters characterizing the solvation response functions and time-resolved anisotropies, composition dependence of viscosity of these melts, and average solvation and rotation times for a dissolved solute in them, and a brief discussion on the theory and relevant equations.
[85]R. Biswas, J. E. Lewis, and M. Maroncelli, Chem. Phys. Lett. **310**, 485 (1999).
[86]H. A. R. Gazi and R. Biswas, J. Phys. Chem. A **115**, 2447 (2011).
[87]Y. Marcus, *Ion Solvation* (John Wiley and Sons Ltd., Chichester, UK, 1985).
[88]C. K. Kim, J. Won, H. S. Kim, Y. S. Kang, H. G. Li, and C. K. Kim, J. Comput. Chem. **22**, 827 (2001).
[89]T. Pradhan, P. Ghoshal, and R. Biswas, J. Phys. Chem. A **112**, 915 (2008).
[90]R. S. Fee and M. Maroncelli, Chem. Phys. **183**, 235 (1994).
[91]M. Maroncelli, private communication (2011).
[92]M. Maroncelli and G. R. Fleming, J. Chem. Phys. **86**, 6221 (1987).
[93]H. Shirota and E. W. Castner, Jr., J. Am. Chem. Soc. **123**, 12877 (2001).
[94]Y. J. Chang and E. W. Castner, Jr., J. Phys. Chem. **98**, 9712 (1994).
[95]R. Biswas and B. Bagchi, J. Phys. Chem. **100**, 1238 (1996).
[96]R. Biswas and B. Bagchi, J. Phys. Chem. **103**, 2495 (1999).
[97]H. Kashyap, T. Pradhan, and R. Biswas, J. Chem. Phys. **125**, 174506 (2006).
[98]S. Roy and B. Bagchi, J. Chem. Phys. **99**, 9938 (1993).
[99]D. Huppert, V. Ittah, and M. Kosower, Chem. Phys. Lett. **195**, 37 (1992).
[100]P. Eberspacher, E. Wismerth, R. Buchner, and J. Barthel, J. Mol. Liq. **129**, 3 (2006); J. Barthel, H. Hetzenauer, and R. Buchner, Ber. Bunsen-Ges. Phys. Chem. **96**, 1424 (1992).
[101]W. W. Rudolph, G. Irmer, and G. T. Hefter, Phys. Chem. Chem. Phys. **5**, 5253 (2003); R. Buchner, T. Chen, and G. Hefter, J. Phys. Chem. B **108**, 2365 (2004); R. Buchner, G. T. Hefter, and P. M. May, J. Phys. Chem. A **103**, 1 (1999).
[102]M. Delsignore, H. Farber, and S. Petrucci, J. Phys. Chem. **89**, 4968 (1985); **90**, 66 (1986); M. Saloman, M. Uchiyama, M. Xu, and S. Petrucci, *ibid.* **93**, 4374 (1989); S. Petrucci and M. Eyring, *ibid.* **95**, 1731 (1991).
[103]J. T. Edward, J. Chem. Edu. **47**, 261 (1970).
[104]R. D. Shanon, Acta. Cryst. **A32**, 751 (1976).
[105]W. L. Masterton, D. Bolocofsky, and T. P. Lee, J. Phys. Chem. **75**, 2809 (1971).
[106]C. G. Gray and K. E. Gubbins, *Theory of Molecular Fluids* (Clarendon, Oxford, 1984), Vol. I.
[107]P. Attard, Phys. Rev. E **48**, 3604 (1993).
[108]A. Chandra and B. Bagchi, J. Chem. Phys. **110**, 10024 (1999); B. Bagchi, Annu. Rev. Phys. Chem. **40**, 115 (1989).
[109]J. L. Lebowitz, Phys. Rev. **133**, A895 (1964).
[110](a) B. Bagchi and A. Chandra, Adv. Chem. Phys. **80**, 1 (1991); (b) J. Barhel, R. Buchner, and B. Wurm, J. Mol. Liq. **98–99**, 51 (2002).
[111]E. Bart, A. Meltsin, and D. Huppert, J. Phys. Chem. **98**, 3295 (1994); **98**, 10819 (1994).
[112]C. F. Chapman and M. Maroncelli, J. Phys. Chem. **95**, 9095 (1991).
[113]E. Neria and A. Nitzan, J. Chem. Phys. **100**, 3855 (1994).
[114]A. Chandra and G. N. Patey, J. Chem. Phys. **100**, 1552 (1994).
[115]A. Chandra, Chem. Phys. Lett. **244**, 314 (1995); A. Chandra, D. Jana, and S. Bhattacharjee, J. Chem. Phys. **104**, 8662 (1996).
[116]A. Voronel, E. Veliyulin, V. Sh. Machavariani, A. Kisliuk, and D. Quitmann, Phys. Rev. Letts. **80**, 2630 (1998).
[117]P. A. Egelstaff, *An Introduction to the Liquid State* (Clarendon, Oxford, 1992).
[118]S. Arzhantsev, H. Jin, G. A. Baker, and M. Maroncelli, J. Phys. Chem. B **111**, 4978 (2007).
[119]N. Balabai and D. H. Waldeck, J. Phys. Chem. B **101**, 2339 (1997).
[120]J. A. Ingram, R. S. Moog, N. Ito, R. Biswas, and M. Maroncelli, J. Phys. Chem. B **107**, 5926 (2003).
[121]N. Ito, S. Arzhantsev, M. Heitz, and M. Maroncelli, J. Phys. Chem. B **108**, 5771 (2004).
[122]A. M. Funston, T. A. Fadeeva, J. F. Wishart, and E. W. Castner, Jr., J. Phys. Chem. B **111**, 4963 (2007).
[123]W. Huang and R. Richert, Phil. Mag. **87**, 371 (2007); J. E. Anderson and R. Ullman, J. Chem. Phys. **47**, 2178 (1967).
[124]K. Santhosh, S. Banerjee, N. Rangaraj, and A. Samanta, J. Phys. Chem. B **114**, 1967 (2010); K. Santhosh and A. Samanta, *ibid.* **114**, 9195 (2010).
[125]Y. Kimura, M. Fukuda, K. Suda, and M. Terazima, J. Phys. Chem. B **114**, 11847 (2010).
[126]K. Ueno and C. A. Angell, J. Phys. Chem. B **115**, 13994 (2011).
[127]M. F. Shlesinger, G. M. Zaslavsky, and J. Klafter, Nature (London) **363**, 31 (1993).
[128]J. Habasaki and K. L. Ngai, J. Chem. Phys. **129**, 194501 (2008).
[129]Z. Hu, X. Huang, H. V. R. Annapureddy, and C. J. Margulis, J. Phys. Chem. B **112**, 7837 (2008).
[130]O. B. Berryman and D. W. Johnson, Chem. Commun. 3143 (2009).
[131]P. Tarakeshwar, S. J. Lee, J. Yong Lee, and S. K. Kim, J. Chem. Phys. **108**, 7217 (1998).
[132]M.-M. Huang, S. Bulut, I. Crossing, and H. Weingartner, J. Chem. Phys. **133**, 10101 (2010).
[133]R. Metzler and J. Klafter, Phys. Rep. **339**, 1 (2000); R. Metzler, E. Barkai, and J. Klafter, Phys. Rev. Lett. **82**, 3563 (1999).
[134]T. Bandyopadhyay, Europhys. Lett. **81**, 16003 (2008); J. Chem. Phys. **128**, 114712 (2008).
[135]T. Pal and R. Biswas, Chem. Phys. Lett. **517**, 180 (2011).
[136]S. Bhattacharyya and B. Bagchi, Phys. Rev. Lett. **89**, 025504 (2002).
[137]S. M. Bhattacharyya, B. Bagchi, and P. G. Wolynes, Proc. Natl. Acad. Sci. U.S.A. **105**, 16077 (2008).
[138]S. M. Bhattacharyya, B. Bagchi, and P. G. Wolynes, J. Chem. Phys. **132**, 104503 (2010).
[139]Y. J. Jung, J. P. Garrahan, and D. Chandler, Phys. Rev. E **69**, 061205 (2004).
[140]J. P. Garrahan and D. Chandler, Phys. Rev. Lett. **89**, 035704 (2002).